5-20-2011

Differential Sedimentation In A Mississippi River Crevasse Splay

Christopher Esposito
University of New Orleans

Differential Sedimentation In A Mississippi River Crevasse Splay

A Thesis

Submitted to the Graduate Faculty of the
University of New Orleans
in partial fulfillment of the
requirements for the degree of

Master of Science
in
Earth and Environmental Sciences

by

Christopher Read Esposito

B.S. Rutgers University, 2003

May, 2011

Acknowledgments

This thesis would not have been possible without the sustained effort of at least a dozen people. Of course my major professor, Dr. Ioannis Georgiou is at the top of the list, having conceived of this project and guided it from its inception. I won't soon forget the many hours that we spent in his office planning this work. My committee members Drs. Alex Kolker and Denise Reed lent their time and their talents to the project in the form of incisive comments and probing questions, and Dr. Kolker collected some of the data that appears in these pages. The best field team that I could have hoped for allowed for two productive field deployments; Kevin Trosclair, Mike Brown, Dallon Weathers, Valerie Cruz, and Duncan FitzGerald, thanks to you all. And a special thanks to Alex Ameen for helping me use some very complicated lab equipment. I would be remiss if I did not thank my radiantly beautiful girlfriend Margaret Davidson, who uttered not one single complaint about my odd hours during these past few months of writing. Perhaps she enjoyed the solitude? And finally my gratitude goes to my father, Gerald Esposito, whose steadfast insistence that I do something interesting with my life seems to have paid off, and to my mother, Sally Ellyson, who put that first pair of binoculars around my neck and made me love science without even using the word.

Contents

List of Figures

List of Tables

Abstract

In this study the patterns of sediment transport and deposition in the channels and receiving basin of a crevasse splay in the modern Mississippi River delta are examined, with emphasis on the development of a distributary mouth bar. Simultaneous hydroacoustic and optical measurements on the mouth bar show that the bar conforms to the progradational stage of an existing conceptual model of mouth bar development. This is confirmed by cores dated using Beryllium-7, which provides a record of the deposition on the bar over a 90-day period. Stratigraphic data from cores obtained on the bar are used to extend the conceptual model to account for variable riverine inputs. A numerical model, developed and validated using field data is capable of representing the fundamental sedimentary processes responsible for mouth bar progradation. These results will be of interest to coastal geologists, engineers and coastal managers alike.

1

Introduction

1.1 Study Significance

In addition to their ecological and economic importance, river deltas worldwide are known to serve as sediment sinks for the material exported from continental interiors (Allison, 1998; Burdige, 2005). The sediment yield and resulting load to the delta, as well as regional and local sediment dynamics within, determine the rate by which land builds vertically and horizontally, or subsides and erodes into the sea. The history of the Mississippi River Delta, including the underlying geological architecture, the volume and age of its deposited sediments, and the conditions in which those sediments were deposited is well known (Roberts, 1997). The cyclic nature of deltaic deposition in the Mississippi River Delta is well documented, as are the frequency of avulsion and river switching events, and the spatial and temporal scales of delta complexes, delta lobes, subdeltas, and crevasse splays (Coleman and Gagliano, 1964). An approximate time scale is associated with each spatial scale of delta deposition; for example a crevasse splay is likely to have a life measured in decades, while a major delta switching event is likely to occur only once in a millennium (Roberts, 1997).

While we understand that these processes occur, we are often unable to say exactly why

they occur in a particular way. For example, as a delta forms, a progression is observed where subaqueous channels and levees form first, then subaerial levees, followed by a full subaerial delta plain. Each step in this sequence is commonly seen, and in fact the full progression has been observed over the course of several decades in the Wax Lake/Atchafalaya system (Van Heerden and Roberts, 1988; Wellner et al., 2005). However, the location of the channels and the timing of events are difficult to predict, and because of the complexity of flows in these systems, only the most general cases can be investigated using hydrodynamic models (Edmonds and Slingerland, 2007). Therefore, in order to accurately predict the behavior of delta systems, it may be necessary to identify the most important parameters and formulate predictive modeling efforts around them.

This study is undertaken as the Mississippi Delta is undergoing rapid submergence (Blum and Roberts, 2009), and as scientists, coastal planners and engineers are struggling to devise methods for maintaining marsh subaereal extent and elevation in the face of rapid rates of relative sea level rise (Morton et al., 2005). One commonly discussed coastal management strategy in South Louisiana is to divert river water and sediments into the wetlands in order to sustain or aid in the growth of existing land (LACPR, 2007). These diversions mimic the functions of crevasses along the lower reaches of the river, many of which are actively depositing sediment and creating small deltas. It is my intention that the ideas and questions addressed herein be used to develop tools that have direct and practical applications for the management of the Mississippi River Delta.

1.2   Mississippi River Delta Cycle

Land building in the Mississippi Delta plain occurs as a series of depositional events that overlap spatially and temporally (Coleman and Gagliano, 1964). The Holocene Mississippi River delta was created in six major delta building episodes, during which were created some

fourteen separately identifiable deltas. Each delta is composed of subdeltas, crevasse splays, and so on, at progressively smaller spatial and temporal scales (Roberts, 1997).

Delta building begins by the infilling of inland lakes, then progresses into bayhead delta building (like the Modern Wax Lake and Atchafalaya deltas), then the active delta progrades across the continental shelf (Tye and Coleman, 1989). The total area of a delta lobe increases until the hydraulic efficiency of its channels decreases to the point that the stream avulses upstream, and another delta begins to form (Roberts, 1997). At this point, the original lobe begins to deteriorate while the new one grows. Avulsion and stream capture from one delta lobe to another is a process that can take centuries, so at any given time there may be more than one active depositional center (Saucier, 1994). The total area of a delta feature at any scale would be the sum of all of its subfeatures

The Wax Lake and Atchafalaya deltas are the fastest growing depositional sites in the Mississippi Delta Plain (Barras et al., 2008). Prior to the rapid growth of the two deltas, the swamps of the Atchafalaya Basin were filled with fine grained swamp deposits, while the lakes were filled with coarser material as the Atchafalaya River's distributaries ran through them (Roberts, 1998). All of this depositional activity has drawn intense study from a geological standpoint (Van Heerden and Roberts, 1988; Allison et al., 2000; Wellner et al., 2005) and from a coastal management standpoint (Mashriqui, 2003; Donnell and Letter, 1992). The Wax Lake Delta in particular has served as a well publicized model for the delta building potential of sediment diversions on the Mississippi River (Kim et al., 2008).

1.3   Land Loss In The Mississippi River Delta Plain

Land loss in the Mississippi Delta has been documented for many years (Gagliano et al., 1981), and the rates and patterns of land loss, as well as the root causes, are still an area of active research (Morton et al., 2005; Barras, 2006; Tornqvist et al., 2006). While many

explanations for the land loss exist, there is consensus that the problem is exacerbated by the hydrologic isolation of the Mississippi River from its floodplain by manmade levees that have been built over the last two centuries.

One often proposed method of managing subsided or submerged wetlands is through the use of planned river diversions to reintroduce river water and sediments into the wetlands (LACPR, 2007; Allison and Meselhe, 2010). The effects of small scale diversions of river water have been examined in terms of their sediment discharge and delivery capacity (Snedden et al., 2007), and the effects of the increased nutrient load on marsh vegetation and soils (Swarzenski et al., 2008; Darby and Turner, 2008). Studies assessing the susceptibility of freshwater soils to shear failure also have implications for diversion schemes (Howes et al., 2010).

Blum and Roberts (2009) calculated the volume of sediment required to sustain the delta in its current configuration, and concluded that a 1mm/yr rise in sea level will result in significant submergence of the existing delta by 2100 unless the delta can capture nearly 100% of the current sediment load in the river. Because 100% capture is impossible, and because 1mm/yr is at the very low edge of the IPCC's predictions for sea level rise (Meehl et al., 2007) , the authors conclude that significant drowning is inevitable, and thus imply that regional planners must acknowledge this fact in their management and restoration plans. The report lacked a clear explanation of the role that organic production plays in maintaining marsh elevation and came under some criticism for that absence (Schleifstein, 2007), but taken as is it serves as a compelling description of the problem and highlights the importance of harnessing the sediment transport capacity of the river to preserve parts of the delta for human use.

A process based[1] numerical model for building land using planned river diversions has

---

[1]The term "process based" refers to a model that captures the broad physical characteristics that are observed in a delta and condenses them into mathematical terms. This is distinct from the type of model that solves the equations of motion to generate a numerical solution, as with Delft3D.

been developed by Kim et al (2007). This model replicates the development and progradation of a fan delta, and is based on observed capture rates in the Wax Lake Delta of 100% for sand and 11% for finer sediments.

1.4   River Deltas

Recent work has demonstrated that the topology of delta channel networks can be predicted under a broad range of conditions (Edmonds and Slingerland, 2007). New methods of measuring bedload in sand bedded rivers have been developed (Nittrouer et al., 2008), and those same studies have suggested that the entire sediment load of the Mississippi River might be in suspension in the outer edges of meander bends. Insights into channel morphology, flow splitting, and sediment distribution in the water column will be used in the modeling portion of the proposed study in order to provide a range of realistic inputs to the hypothetical basins that will be investigated.

Edmonds and Slingerland (2007) point out that while bifurcation is a fundamental process in delta building, the prediction of specific bifurcation geometries and of channel network topology is not possible using any existing conceptual model of delta growth. Their analysis of serial imagery of deltas confirms previous work (Van Heerden and Roberts, 1988) that shows that channels tend to bifurcate around channel mouth bars and then stabilize in the resulting configuration. Thus the ability to predict the location of channel mouth bars would confer the ability to predict the significant features of the forming delta channel network. Edmonds and Slingerland (2007) developed a numerical model, implemented in the Delft3D suite, to simulate the formation of a channel mouth bar as a sediment laden turbulent jet flows into a receiving basin. Their results demonstrate the mechanics of mouth bar formation, progradation, and the cesation of progradation. It is well understood that mouth bars form because a decrease in effluent velocity (due to flow expansion) causes sediment to fall out of

suspension (Wright and Coleman, 1974), and their results suggest that this is most likely to occur between zero and two channel widths basinward of the channel mouth. It is further suggested that mouth bars prograde because the flow is constricted vertically as they aggrade towards the water surface, thereby increasing the velocity and scouring material from the near bar apex to be deposited farther downstream on the bar. The progradation stops when the pressure gradient above the bar is not sufficient to overcome the frictional resistance introduced by the bar, forcing flow into the channels that now flank the bar; this final phase is termed runaway aggradation. The model data presented suggests that progradation stops when the height of the water column over the bar is less than 40% of the channel depth at the inlet. See Figure 1.1 for further details on the conceptual mouth bar model.

Other work by Edmonds and Slingerland (2009) has explored the importance of sediment cohesion (understood to be attributable to grain effects as well as vegetation effects) in a series of numerical experiments. High cohesion scenarios were found to result in elongated, birdsfoot-type, deltas, while low cohesion scenarios were found to result in more fan shaped delta configurations. Adding cohesion to the system creates a competition between levees and mouth bars. Highly cohesive sediments create mouth bars that are difficult to erode, but levees are also strengthened and lengthened, creating a more intense outflow jet that is a more efficient at eroding mouth bars. The highest number of bifurcations comes at some intermediate value where the two effects of the cohesion balance each other out.

Geleynse et al. (2010) have simulated delta complexes using a numerical model that captures the fundamentals of delta stratigraphy and sedimentology, including the development of a fine grained prodelta overlain by sand bodies that fine upwards. Geleynse et al. (2011) extends the earlier model to include the effects of tides and waves on a delta, and show that a numerical model is capable of reproducing the essential characteristics of the various sediment/tide/wave dominated deltas of classic classification schemes (Galloway, 1975). Confirming the results of Edmonds and Slingerland (2009), Geleynse et al. (2011) state that

cohesion (either sediment or vegetation) is found to be a critical control on the presence and degree of delta elongation. They further suggest additional downstream controls on the shape of the delta planform and resulting stratigraphy, most notably tidal forcing.

Most relevant to the Modern Mississippi River delta are studies examining the formation and mechanics or "elongate" deltas (also called "birdsfoot" or sometimes "river-dominated"). Kim et al. (2009) developed a conceptual model of delta growth where a delta with a high mud (cohesive) content is able to prograde into a low energy basin in such a way that the effective sediment source prograde downstream with the channel levees. They suggest that this type of mechanism is responsible for the elongated region of the lower Mississippi River delta and that the birdsfoot region formed when the increased slopes of the continental shelf disrupted the progradation of the levees, allowing sediment to be distributed laterally through coastal processes. These results agree with Edmonds and Slingerland's conclusions that increased cohesion is the key to creating elongated deltas.

Seybold et al. (2009) take a unique approach to the problem by developing what is called a "reduced complexity model" of delta growth. Reduced complexity in that the model does not rely upon the well known equations of fluid dynamics, but rather on a set of rules evaluated at each cell across a domain, and then tuned to provide realistic results. The model coefficients must be tuned during calibration and are not transferable to other systems, representing a limitation to this method of delta simulation.

Hoyal and Sheets (2009) were able to simulate birdfoot deltas in a physical model by adding a cohesive polymer to their sediment mixture. Using these models they were able to identify several cycles that are important to delta growth. The bar cycle, also examined by Edmonds and Slingerland, is the most rapid cycle, followed by an avulsion cycle that occurs when multiple bar cycles result in a morphodynamic backwater effect and eventually channel avulsion. The longest cycle is the delta cycle, often discussed in literature (Roberts, 1997; Coleman and Gagliano, 1964). The avulsion cycle (in Roberts' terminology this would be

the Subdelta Cycle) is further subdivided into three stages: a stage where channel extension occurs via incision and levee elongation (the positive feedback stage), a stage where bar aggradation takes effect and the morphodynamic backwater effect begins to take on increased importance (the negative feedback stage), and finally an upstream avulsion stage where the river avulses into a path with a more favorable gradient.

1.5   The Sediments of the Lower Mississippi River

Horowitz (2010) and Kesel (1988) both report persistent declining trends in the mass of suspended sediment fluxes in the Mississippi River. Kesel (1988) reported that the average suspended sediment load over a 25 year span ending in 1988 is 1.4×10^8 metric tons/yr. This translates to 3.84×10^5 metric tons/day on average, which is of the same order as the total suspended loads reported by Allison (2009) during field survey conducted in 2008 and 2009. Allison (2009) reports suspended sediment load in two classes: sand (> 63 microns) with a peak load of 10^5 tons/day, and mud (< 63 microns) with a peak load of 2.8×10^5 tons/day were recorded during April of 2009. The minimum numbers, recorded at low water during October of 2008 were approximately 10^3 tons/day of sand and 1.2×10^5 tons/day of mud. It is important to emphasize that the numbers reported by Kesel are long term averages while the numbers of Allison are discrete measurements during a single flood season, so comparisons between the two are difficult to make.

Nittrouer et al. (2008), in the absence of readily available bedload measurements, developed a unique methodology and reported a "bedform sand transport" of approximately 2.2×10^6 tons/year. This method is based on repeated multibeam bathymetry surveys of four reaches between New Orleans and Head of Passes, using a multibeam sonar system. Their results show that the bedform transport rates increase exponentially with river discharge, and that a significant fraction of river sand is in suspension during high flows. Allison (2009)

reported sand in suspension throughout the water column at locations between River Miles 46 and 26. In some cases the sand concentration exceeded 30mg/l at 10% of the water depth (the shallowest measurements taken). The presence of significant quantities of sand in suspension, and particularly near the surface of the water column, is important to the present study.
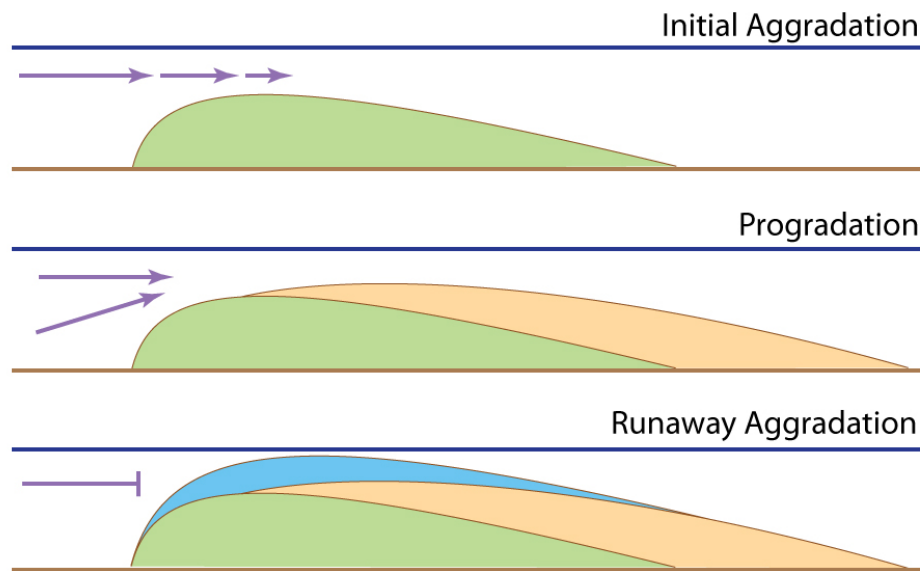
Figure 1.1: The Edmonds and Slingerland (2007) model for mouth bar growth. An initial aggradation stage commences as a turbulent, sediment laden outflow jet expands in a receiving basin, reducing jet velocities and causing deposition. As the bar grows, flow is vertically constricted above the bar, causing bar top velocities to increase. The increased bar top velocities result in a progradation phase, when material is then scoured from the top of the bar and deposited at the distal end of the bar. Finally, as the flow resistance on the bar grows, the flow bifurcates and flows through the channels that surround the bar. Velocity is severely reduced on the bar top due to lack of fluvial input, and suspended sediments deposit quickly; the bar is now in a runaway aggrational phase and grows vertically to the water surface.

2

Research Plan

2.1 Study Description

The study described herein was designed with the goal of linking river channel processes with sediment transport and deposition in the channels and wetlands of the river delta. The mouth bar that is studied is more than 5 km from the main channel of the Mississippi River, and flow from the river must pass through five bifurcations and one confluence before arriving there. The fact that such a long and complicated channel network is feeding a feature that is actively growing at an inland location makes this site an ideal location to study the processes of channelized sediment transport and deposition in a deltaic environment distinct from the river mouth.

The work presented in this manuscript represents an effort to capture the essential sediment dynamics of a small natural delta system and test the results against current theory, particularly the theory pertaining to the development and function of distributary mouth bars, which have not been widely examined in the field using modern methods. Further attention will be given to developing and calibrating a numerical model of the system which can be used to examine the response under a range of inputs and forcing conditions.

2.2   Study Goals

The goals of this study are as follows.

1. To collect data in an actively growing crevasse splay that can be analyzed to provide a clear picture of the hydrodynamic and sediment transport behavior of the system.

2. Place observations of an evolving distributary mouth bar in the context of current conceptual models.

3. Extend the conceptual model to account for the full set of field observations.

4. Use the field observations to develop a numerical model which can be used to evaluate the splay's behavior under a range of possible scenarios.

5. Use the lessons learned from this system to develop a framework for assessing river diversion restoration schemes, and the conditions under which they may be successful.

2.3   Primary Hypotheses

1. Observations of an evolving distributary mouth bar will conform to the three stage conceptual model advanced by Edmonds and Slingerland (2007).

2. A numerical model can be developed that will capture the fundamental patterns of sediment transport and deposition on a distributary mouth bar. This initial surface for this model should represent the actual shape of the mouth bar, and the model should be initialized and calibrated with in situ data from an existing mouth bar and from the main channel of the Mississippi River.

2.4   Study Site

Figure 2.1: Aerial imagery from 2008 showing a regional view of the Cubits Gap distributary network. Brant's Pass, formed in 1975, is circled in blue, and is shown in detail in Figure 2.2. The image is from Atlas (2008).

This study takes place in the Brant's Bayou Splay within the Cubit's Gap Subdelta. Cubit's Gap is a subdelta of the modern Mississippi River Delta, also known as the Balize delta lobe (Roberts, 1997). The Balize subdelta has been active for more than 1000 years, during which time it has filled the accommodation space between the St. Bernard and Lafourche delta lobes and prograded to the edge of the continental shelf. Because of its location on the steeply sloping shelf edge the Balize subdelta has deposited a thicker sediment package than the other subdeltas, and is therefore uniquely prone to subsidence from compaction (Yuill et al., 2009).
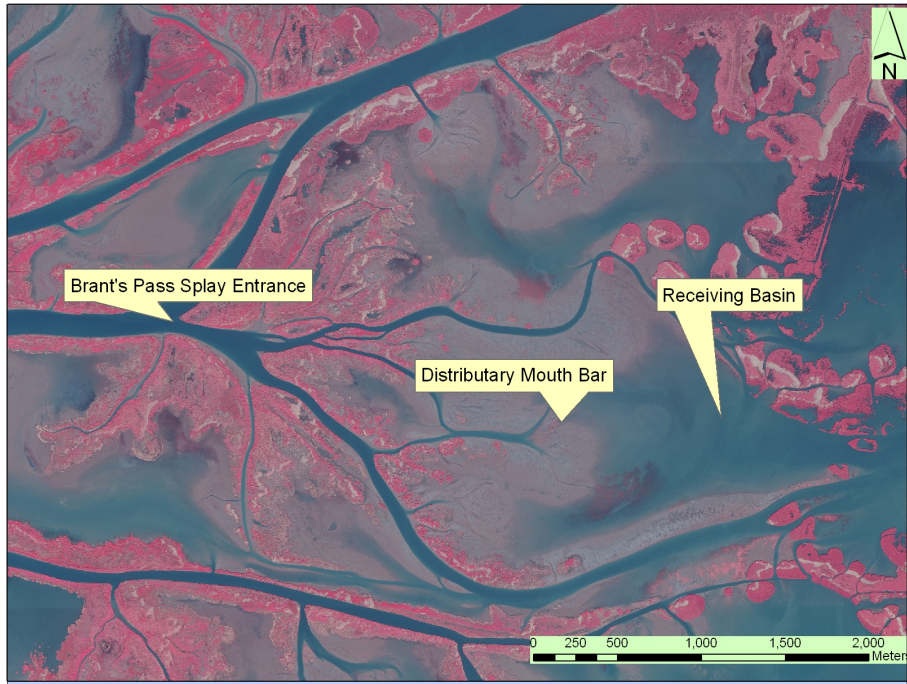
Figure 2.2: Detailed view of the Brant's Pass Splay showing the entrance from the main distributary channel, the distributary mouth bar examined in this thesis, and the receiving basin into which the mouth bar progrades. Extensive mudflats can be seen upstream of the mouth bar and along the major splay channels to the North and South of the mouth bar. The image is from Atlas (2008)

Cubit's Gap was formed in 1862 as a manmade cut in the levee on the left bank, approximately 12 km below Venice, LA. Between 1862 and the 1940s, the splay created nearly 200 km^2 of subaerial land, and has been in a declining phase ever since (Welder, 1959). Despite the decline in land area, the Cubit's Gap distributary network remains robust and carries approximately the same fraction of the river (12%) as it did a century ago (Allison, 2009; Welder, 1959). Persistant high rates of subsidence facilitated the transformation of land to open water ponds. The transformation resulted in an increase in energy gradient between the channels and the ponds and an increase in vertical accommodation space, thereby creating favorable conditions for levee breaching, especially during high flow events. The study site was formed when the right levee of Brant's Bayou, one of the Cubit's Gap distributaries,

14

failed during the 1975 flood (Roberts, 1997).

The resulting splay has built a delta into a large subsided pond that was previously a robust marsh when the Cubit's Gap subdelta was at its largest, and was a more active depositional system. Prior to the opening of Cubit's Gap this area would have been an open water bay called Bay Rondo (Roberts, 1997). Thus an observer at the site of the current splay since 1860 would have observed open water, then subaerial marsh as the Cubit's Gap subdelta prograded across the area, then open water once more as the original Cubit's Gap marshes subsided and ponded, and finally subaerial marsh again as the current splay prograded into the pond. Eventually the observer will see the area return to open water as the splay exhausts its life and as the entire region subsides.

The current configuration of the splay resembles that of a fan-shaped delta with a subaerial radius of approximately 1.5km, flowing into an irregularly shaped receiving basin that has major and minor axes of approximately 4 and 3km, respectively. On the fringes of the delta and along the levees of some channels are extensive mudflats. Other large mudflats also exist near the center of the basin as an active distributary mouth bar. Channels and runnels evident in satellite imagery appear to indicate overbank flow on all of the mudflats.

The fan-shaped part of the delta is heavily vegetated, and the vegetative succession pattern of this location is described by White (1993). On the fully developed islands of the upper parts of the splay the most upstream part of the island is also the highest, and is dominated by Salix nigra (black willow). Further downstream the mudflats and slightly submerged areas are dominated by Scirpus deltarum (bulrush)[1] , with the intermediate elevations home to Colocasia esculenta (elephant ears). During the high water deployment (April, 2010) the mouth bar that serves as the focus for this study was covered by clumps of senesced cane-like vegetation. These were probably S. deltarum, which were seen flourishing

---

[1]Our observations in the field were that phragmites dominated at almost all locations except for the dynamic environment of the mouth bar. An invasive phragmites outbreak is ongoing in the area (Personal Communication, David White), lending credibility to these observations.

in the same location during the low water deployment (November 2010). At low water, large mats of water hyacinth were seen stranded on the mouth bar and choking the channels surrounding the mouth bar and floating in small (1-1.5m) clumps throughout the splay.

By 1993 the splay had a well developed channel network that has remained essentially stable to the present.[2] The feature continues to grow rapidly, with a USGS report assessing a 40% increase in subaerial extent between 2002 and 2008 (USGS, 2005, 2009) (see Figures 2.3(a) and 2.3(b)). This growth is observed despite the fact that the two largest channels in the system have prograded beyond the edge of the receiving basin and thus the bulk of their sediment load is lost to the splay system.

---

[2]These channels were probably developed in their current configuration earlier than 1993, though imagery to show that is not available. There is a 1983 image is shown in (White, 1993) that might show the channels in their current locations, but the document scan is of poor quality and we cannot know for certain without a better image.
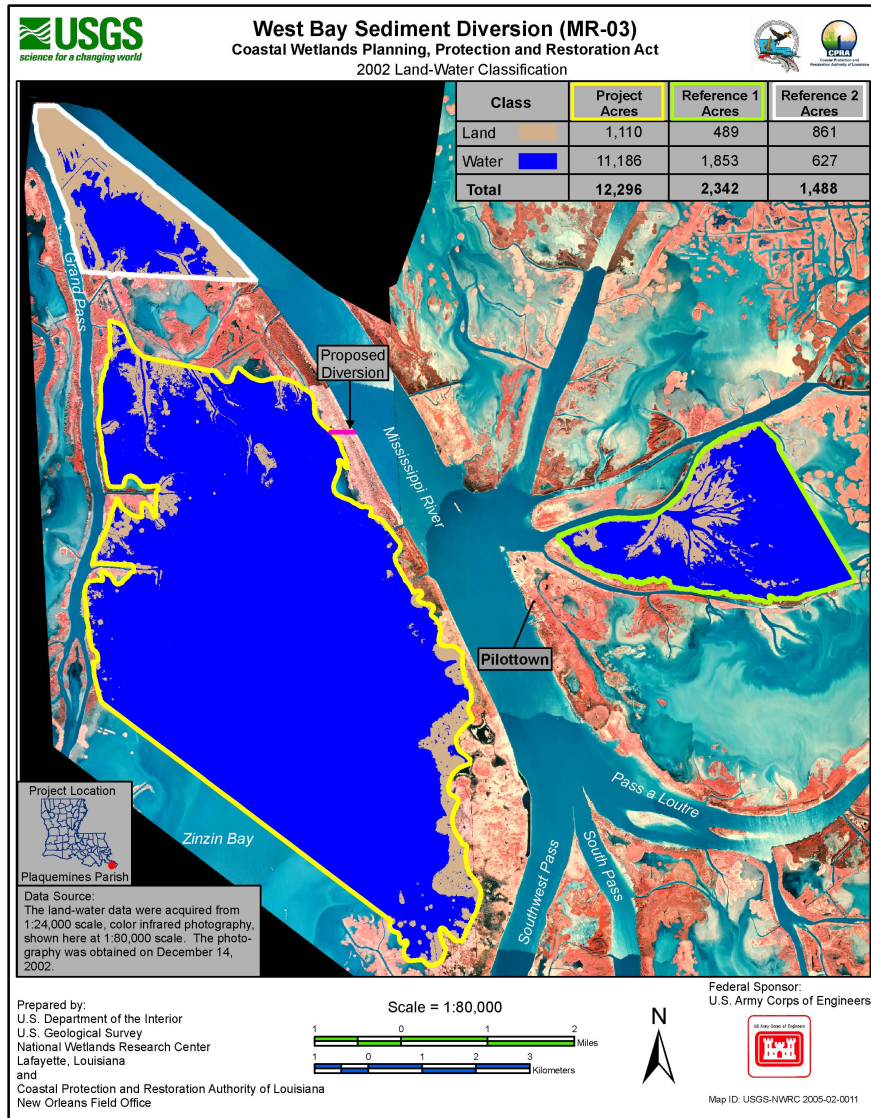
(a) Land area measured in 2002 (USGS, 2005).

Figure 2.3: Land Area Analysis

West Bay Sediment Diversion (MR-03)
Coastal Wetlands Planning, Protection and Restoration Act
2008 Land-Water Classification

Class		Project Acres	Reference 1 Acres	Reference 2 Acres
Land		1,493	680	844
Water		10,803	1,662	644
Total		12,296	2,342	1,488

Grand Pass

Main Pass

Diversion
completed
November 6, 2003

Mississippi River

Pilottown

Pass a Loutre

Project Location

Plaquemines Parish

Zinzin Bay

Southwest Pass

South Pass

Data Source:
The land-water data were obtained from digital imagery (Z/I Imaging digital mapping camera) with 1-meter resolution acquired October 27, 2008. All areas characterized by emergent vegetation, wetland forest, scrub-shrub, and upland were classified as land, while open water, mud flats, and aquatic beds were classified as water.

Scale = 1:80,000

0.9   0   0.9   1.8 Miles

0.9   0   0.9   1.8   2.7 Kilometers

N

Prepared by:
U.S. Department of the Interior
U.S. Geological Survey
National Wetlands Research Center
Lafayette, Louisiana
and
Coastal Protection and Restoration Authority of Louisiana
New Orleans Field Office

Federal Sponsor:
U.S. Army Corps of Engineers

Map ID: USGS-NWRC 2009-02-0315

(b) Land area measured in 2008. The area of subaerial land in Reference Area 1 has increased by 39% (USGS, 2009).

Figure 2.3: Land Area Analysis. (cont.)

3

Field Methods

Two field expeditions were made to the Brant's Pass Splay using UNO's research vessels R/V Mudlump and R/V Ratcrud, and LUMCON's R/V Safe Boat. In order to investigate the sedimentary and flow processes at the study site during two distinctly different flow regimes the first deployment, in April of 2010, was timed to coincide with the peak spring flood flows in the Mississippi River while the second, in November of 2010, coincided with the lowest river flows of the year (see Figure 3.1).

3.1   ADCP

A ship mounted RDI Rio Grande Workhorse 1200KHz Accoustic Doppler Current Profiler (ADCP) was used to survey the flows at selected transects throughout the splay and the network of channels that feed it. During the April deployment, ADCP data was collected at the mouth of each selected channel, and upstream of each bifurcation. The data taken upstream of each bifurcation served to ensure flow continuity through the bifurcation. Figure 3.2 shows the locations of each ADCP transect taken along the path from the river to the mouth bar during the April Deployment.
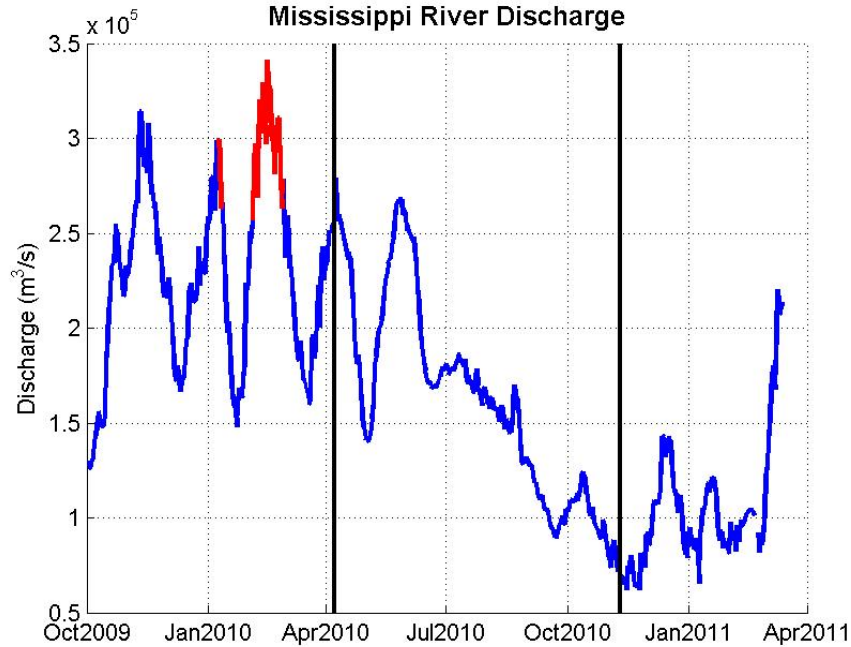
Figure 3.1: Mississippi River discharge measured at Belle Chasse, Louisiana. Vertical lines mark the dates of the two field deployments. Peak discharge days between January 7 and April 7 shown in red. Peak days are defined to be days in which discharge met or exceeded the discharge measured on April 7. There are 32 peak discharge days.

The ADCP operates by sending a measured pulse of sound into the water column. The sound pulse bounces off of particles entrained in the water column and is returned to the instrument. The Doppler shift between the transmitted and the returned sound waves is used to determine the speed of the water relative to the instrument. Those velocities are accumulated into a cross section and multiplied by the appropriate area to give the measured flow through the cross section. The ADCP is unable to measure velocities at the very top or the very bottom of the water column, or at the shallow areas at the edges. For these areas the ADCP software (WinRiver II) is able to extrapolate a velocity profile in order to calculate the flow. The flows reported herein are the sums of the total measured flow along a cross section plus the extrapolated flows at the top, bottom, and sides (Teledyne RD Instruments, 2007). Extrapolation of the top, bottom, and edges represents a possible

source of error in the ADCP flow data.

An attempt was made to survey each transect shown in figure 3.2, however the survey boat was not able to access locations 4.1, 4.2, 4a, 5.1 or 5.2. Each transect that was surveyed was surveyed at least twice, with the exception of location 3.2, which was only surveyed once. The percent error between flow measurements at a single location was never more than 2% from the mean flow at that location. Because of the consistency among transects taken at the same location, and because flows tend to add together as expected (e.g. the flows at 3.2 and 3.3 sum to the flow at 2b), I have high confidence that these data consistently represent the flows in the channel.

Although the data taken in each channel is consistent with other measurements in the same channel, it is also likely that the velocities that were recorded, and therefore the flows, underestimate the true conditions. ADCPs are prone to "moving bed error" which results when the instrument attempts to use the bed as a constant reference location but the bed itself is moving either as fluid mud or large numbers of saltating grains (Mueller and Wagner, 2009). Because the bed is moving in the same direction as the current, using the bed as a reference makes it appear that the water is moving less quickly than it really is. The best way to avoid this type of error is to take spatial reference information from a high quality GPS system, but because of an equipment failure we were forced to use the bed as a reference. The end result is that all velocities and flows must be biased slightly down by an unknown factor. Because the velocities are consistent throughout the splay the bed is likely moving at a similar speed at all locations(see Figures 4.1(a) - 4.1(h) in the Field Results and Discussion chapter), and therefore the factor is assumed not to vary with transect location.

Figure 3.2: ADCP data is shown from the channel sites indicated.

3.2   LISST and ADV

A Sequoia Scientific Laser In-Situ Scattering and Transmissometry (LISST) particle size analyzer was used in concert with a Nortek Vector 6MHz Acoustic Doppler Velocimeter (ADV) to obtain simultaneous suspended sediment and velocity measurements at locations throughout the splay receiving basin. Data were obtained in two transects on the mouth bar, both running from the apex of the bar to the distal edge where the deeper basin waters begin (see Figure 3.3). These transects were selected in the field so that data would be obtained along flow streamlines. Further data points were taken in the basin between the mouth bar and the outflow point for the splay in order to collect velocities in the receiving basin, and to observe the velocity gradient downstream of the bar. All suspended sediment sizes here taken using water pumped from 12 inches above bed level. The water was pumped
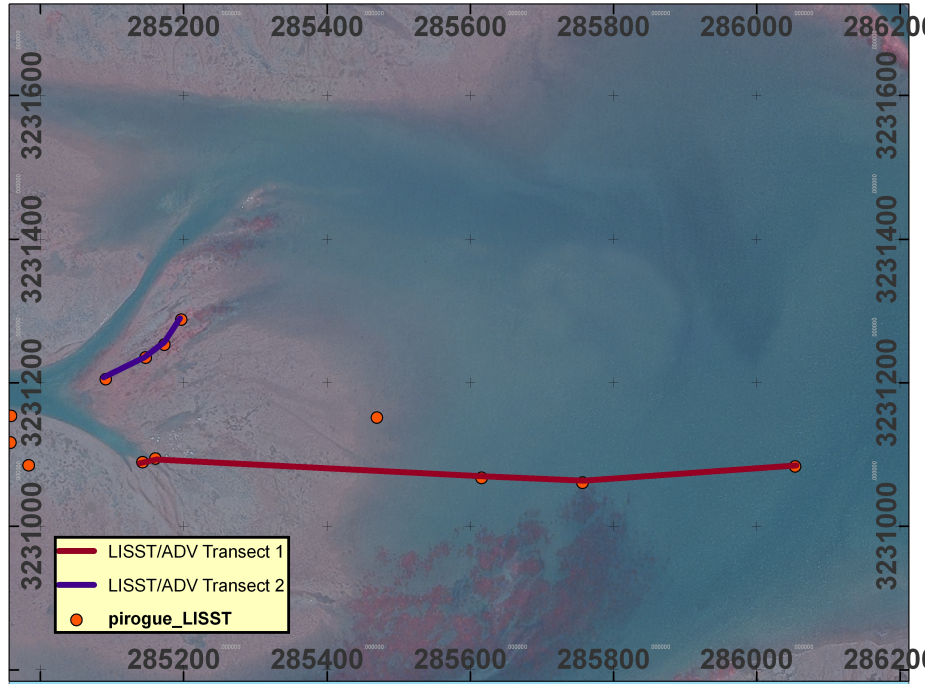
Figure 3.3: Detail of the mouth bar, showing the locations of the suspended sediment (LISST) and velocity (ADV) measurements shown in Figures 4.2 and 4.3

to the surface using a pump that pulled the water through the LISST's testing chamber. The pump itself was situated after the testing chamber so that the sediments were unaffected by the mechanical action of the pump until after they were analyzed. This method minimized the disturbance to flocculated or otherwise aggregated suspended particles. The ADV was mounted on a pole for stability and used to evaluate water velocities at 15 cm above the bed.

The LISST obtains the size of the sediments in the water by measuring the angle of diffraction of laser light as i passes through the sample. Because - contrary to the name of the instrument - it is the angle of diffraction that is used to determine the size of the sediment particles, the results are independent of the material composition of the particles themselves. Thus the LISST can be used in open ocean waters where biological particles dominate as well

as in turbid streams where mineral sediments are the most plentiful suspended constituent (Sequoia, 2007). One drawback of the laser diffraction data is that all particles are assumed to be spheres[1]. This assumption becomes increasingly erroneous with decreasing particle size, which must be considered when comparing LISST data with other sediment measurements derived from methods other than laser diffraction.

The ADV is similar to the ADCP in that it uses sound pulses and the Doppler effect to evaluate water velocities, however the ADV returns high frequency (4 - 64 Hz) velocity readings of the water in a very small volume (9 - 35 cm^3) rather than in the entire water column (Nortek, 2005). The ADV returns a 3-Dimensional velocity vector, which was decomposed into its components. The locations of LISST and ADV samples can be seen in figure 3.3.

3.3 Bottom Samples and Cores

The location of all bottom sediment samples obtained can be seen in Figure 4.6(a). Channel bottom samples were obtained at the beginning and the end of each channel reach, as defined by bifurcations and confluences. Additional samples were obtained along the main feeder channel to the splay between Locations 2.3 and 2a. and along the North and South channels of the splay. Additional bottom samples were obtained along Transects 1 and 2 shown in Figure 3.3, and from the short cores shown in Figure 4.4.

During the April 2010 spring flood, sixteen short cores were collected on and around the mouth bar(Figure 4.4), and each was sampled for Beryllium-7 (^{7}Be) at 0.5, 1.5, and 2.5 cm using the methods detailed in Feng et al. (1999). ^{7}Be has a 53.3 day halflife, and approximately 30% of its mass will remain after 90 days. Thus, the presence of ^{7}Be is taken to indicate deposition within the previous 90 days. Of the sixteen cores collected and

---

[1]Sequoia actually does offer an option to consider randomly shaped particles, and claims that results from this method are more accurate. However, I have not had the opportunity to evaluate the results using the "random" option, and all results reported herein assume the particles to be spherical.

sampled, eight showed the presence of Beryllium in each of the depths and three showed Beryllium to 1.5 cm. This means that three of the sites sampled received a minimum of 1.5 cm of new sediments deposited over the 90 days prior to April 7, 2010, and eight sites received a minimum of 3 cm over that same time. The cores were only sampled down to 2.5 cm, so the full extent of the sedimentation is not known. One core (CB15) is not considered here because ^{7}Be was detected in the second cm but not on the surface, possibly indicating a sample that was disturbed during collection.

Longer (0.5 and 1 m) cores were taken on the mouth bar during the November deployment using a Russian peat corer. Due to difficult and unexpected field conditions, only core locations closest to the channel could be obtained. Core locations are shown in Figure 4.8.

3.4   Bathymetry

During the November 2010 deployment, channel bathymetries of the splay and its main feeder channel were taken using an Odom Hydrotrac 200kHz transducer with a TSS DMS-25 motion reference unit to remove boat motion noise. The Hypack software suite was used for data acquisition and processing, and spatial reference was provided with a Thales Zmax.NET dual frequency GPS.

4

Field Results and Discussion

4.1 Water and Sediment Capacity of Splay Channels

Examination of the ADCP data shows the distribution of flow within the splay (Figure 4.1). The splay itself (Channel 2b in Figure 4.1) takes nearly 10% of the flow entering Cubit's Gap from the Mississippi River. The flow splits nearly evenly at the first bifurcation (3.3/3.4), and then asymmetrically at the subsequent bifurcation in each channel (4.1/4.2 in the North Channel and 4.3/4.4 in the South Channel). Channel 4.3 takes less than 1% of the flow at Cubit's Gap, and while Channel 4.2 was inaccessible at the time of the April survey it is likely to carry a similar flow, considering that the width of the channel is similar to that of channel 4.3. The flow at the apex of the mouth bar is therefore estimated to be on the order off 2 - 2.5% of the Cubit's Gap flow, or 60-70m^3/s. See Table 4.1 for flows recorded at each surveyed channel.

The depositional site in this case is over 5km from the source of its water and sediment, so a critical part of understanding why the observed splay feature occurs here but not elsewhere is to understand the transport capacity of the channel network leading to, and inside of, the splay. To this end, the ADCP transects were also examined to assess the
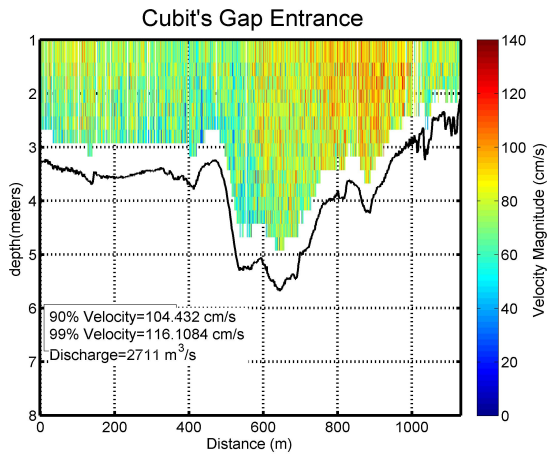
(a) Location 1 in Figure 3.2
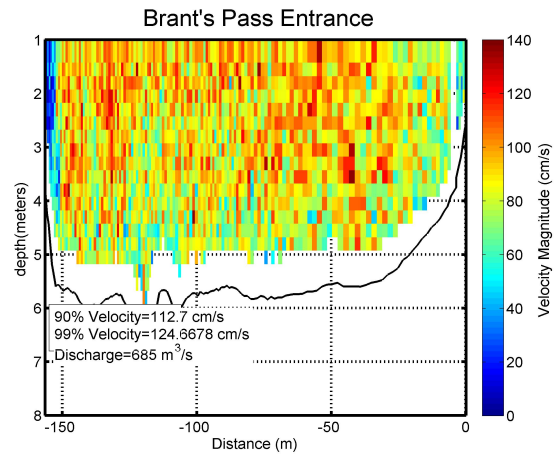
(b) Location 2.3 in Figure 3.2
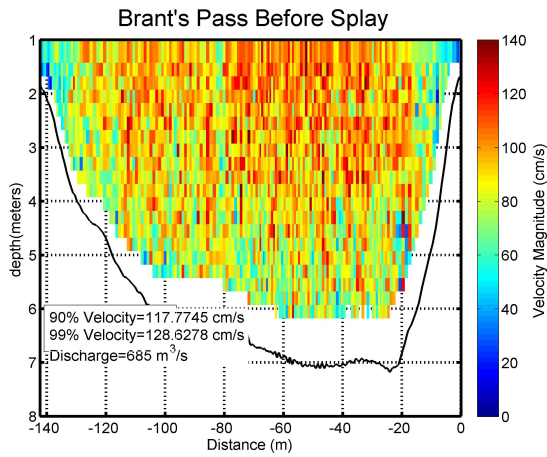
(c) Location 2a in Figure 3.2
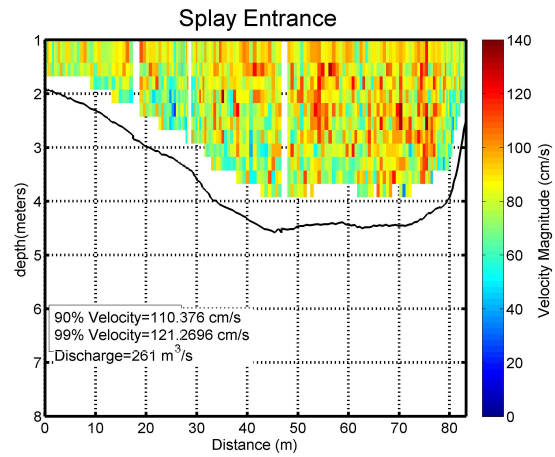
(d) Location 2b in Figure 3.2

Figure 4.1: ADCP cross sections.
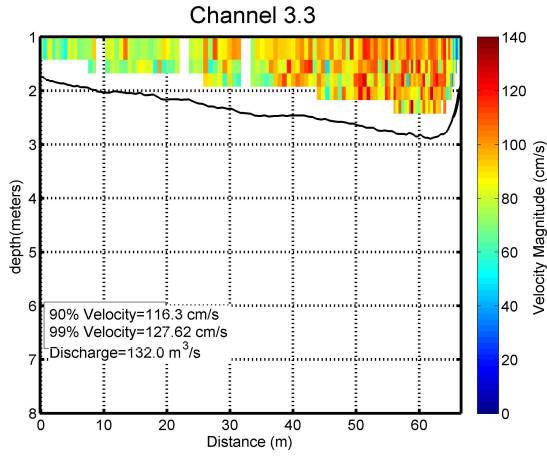
(e) Channel 3.3
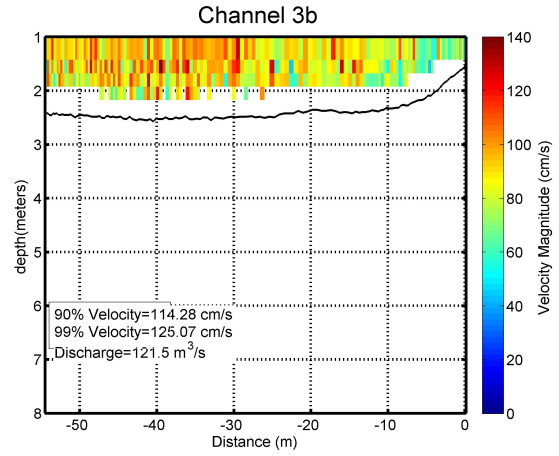
(f) Channel 3b
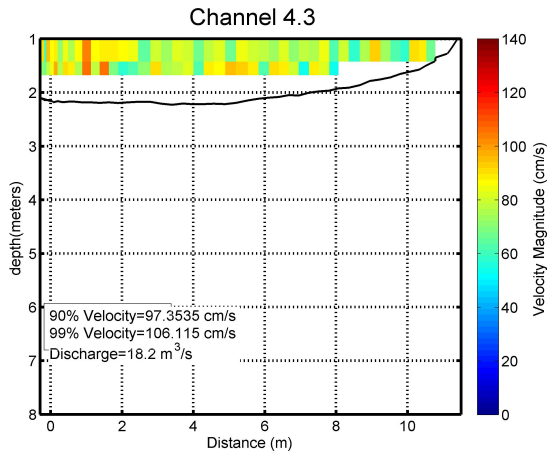
(g) Channel 4.3
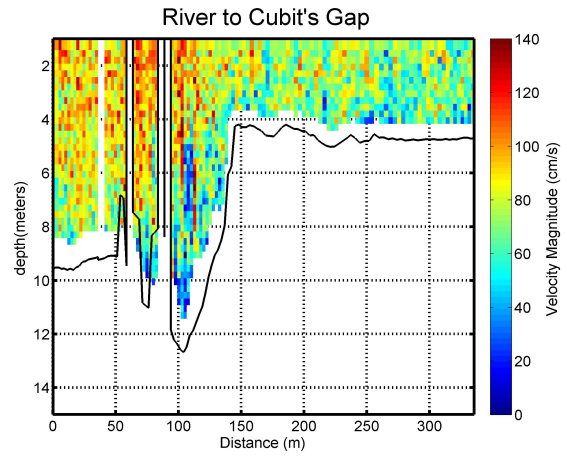
(h) River to Cubit's Gap. This section shows the steep slope of the channel side, making bed transport from the river into Cubit's Gap impossible.

Figure 4.1: ADCP cross sections. (cont)

Location	Flow ($\frac{m^3}{s}$)	%CG Flow	Hydraulic Radius (m)	Surface Slope	U*	Rouse Number
1	2711.00	100.00%	4.00	3.68E-05	3.80E-02	1.33
2.3	685.00	25.27%	4.30	3.68E-05	3.85E-02	1.28
2b	261.00	9.63%	2.19	8.58E-05	4.33E-02	1.18
3.3	132.00	4.87%	1.80	8.58E-05	3.89E-02	1.37
4.3	18.15	0.67%	1.05	9.70E-05	3.16E-02	1.60
2b, Nov	39.00	6.22%	NA	NA	NA	NA
1, Nov	626.75	100.00%	NA	NA	NA	NA

Table 4.1: ADCP data showing the discharge and sediment transport conditions through each channel leading to the mouth bar. Notice that, despite variation in flow, slope, and hydraulic radius, the Rouse Number is consistent throughout the system.

sediment carrying capacity of the channel network that feeds the splay. We first notice that while the cross sectional velocity distribution is noticeably different between channels (some channels have a clearly defined high velocity core, while others have a nearly uniform velocity cross section) the upper limit of the velocities is consistent throughout the splay. The 90-99th percentile velocity magnitudes was extracted from each transect and is shown in figures 4.1. It is apparent that the highest velocities (excluding the highest 1%) are in the 110-130cm/s range throughout most of the splay. This analysis includes the entrance to Cubit's Gap at the Mississippi River, so we are able to conclude that any sediments that are introduced to Cubit's Gap in suspension (e.g. the velocities at the Cubit's Gap entrance are sufficient to keep the sediments in suspension) can be transported throughout the splay by the velocities observed in the channels. One exception to this conclusion are the velocities observed in Channel 4.3, which is the last channel that was able to be surveyed upstream of the mouth bar. The highest velocities observed in this channel are noticeably lower than the 110-130 cm/s range observed in the upstream channels, however an assessment based on Rouse Numbers (see below) places this channel in the same range as the others with respect to its ability to transport the coarsest material observed in the splay system.

Reach	Surface Slope
Prior To Splay	3.68E-05
Upper Splay	8.52E-05
Lower Splay	9.70E-05

Table 4.2: Three distinct slope regimes were observed between the entrance to Cubit's Gap and the mouth bar. A gradient change occurs upon entering the splay, and again upon entering the final channels prior to the mouth bar. The transition from Channel 3.3 to 4.3 (see Figure 3.2 marks the transition from upper to lower splay regimes.)

Another way of assessing the transport capacity of a channel or reach is by computing the Rouse Number. The Rouse Number is the ratio of the fall velocity of a particle to the shear velocity of the water column.

$$N_R = \frac{V_o}{kU^*}, \tag{4.1}$$

where $k = 0.4$ is Von Karman's constant and $U*$ is the shear velocity, defined as the average per channel reach, as shown in Babaeyan-Koopaei et al. (2002) .

$$\bar{U}^* = \sqrt{gRS_f} \tag{4.2}$$

Here, R is the hydraulic radius of the channel, and S_f is the surface slope. The hydraulic radius is defined as the ratio of the cross sectional area of a channel to its wetted perimeter, and was calculated with the depths collected during the ADCP survey. The surface slopes were estimated using continuous DGPS data (with vertical control and accuracy) recorded during the ADCP survey. Three different water surface slope regimes were observed, with the slopes generally increasing with distance from the river as the channels narrowed and frictional effects increased in importance. Water surface slopes were lowest in the channel that led to the splay, increased markedly inside the splay, and then increased slightly again in the final channels leading to the mouth bar. Fall velocities were calculated using Stokes'

Law for 150 μm quartz particles, which is in the range of the coarsest sands seen in the bed materials of the splay. Stokes' law states that it's fall velocity can be calculated as

$$V_o = \frac{1}{18}\frac{(\sigma - \rho)gD^2}{\eta}, \tag{4.3}$$

for a particle of diameter D and density σ in a fluid of density ρ and viscosity η.

The calculated Rouse Numbers can be seen in table 4.1. As with the velocities, the Rouse Number remains consistent along the channel network leading to the mouth bar, with values between 1.3 and 1.6. According to Whipple (2004) , Rouse Numbers in this range indicate that approximately 50% of this sediment is expected to be in suspension at a given time.

4.2   Sediment Transport on the Mouth Bar

Edmonds and Slingerland (2007) demonstrated numerically the existence of a critical water depth necessary for vertical aggradation of a mouth bar. Once the bar aggrades such that the water depth above the bar is shallower than the critical depth, flow over the bar is constricted vertically and accelerated, causing bar-top sediments to be transported downstream and deposited at the distal end of the mouth bar. Thus, aggradation ceases, rendering down-basin progradation the dominant depositional process.

Simultaneous, co-located measurements of suspended sediment and velocity were collected along Transect 2 (see Figure 3.3) on the mouth bar. Transect 2 begins at the apex of the mouth bar and proceeds downstream along the flow streamlines towards the receiving basin. Figure 4.3 shows that the flow velocity over the mouth bar remains stable at 25 cm/s for more than 100m, then increases to a peak of near 50 cm/s near 165m, then falls back below 30 cm/s on the more distal regions of the bar. As the flow increases, so do the size and volume of sediments suspended in the water column. Because the water flowing over the bar at the more upstream locations is clearer (i.e. the volume of suspended sediment is less),

and because the character of the suspended sediment is fundamentally different (as can be seen in the median grain size), it can be concluded that the additional sediment suspended in the water column must have been scoured from the bed.

Similar data were collected along Transect 1 (Figure 4.2), beginning on the mouth bar and running towards the basin outlet. In this case the mean velocity, grain size, and suspended sediment volume all decrease in tandem as the sediment laden water slows down and drops its sediment load in the receiving basin. There is a small increase in velocity towards the end of the transect as flow constricts to leave the basin through its outlet but no resuspension of sediment is evident in the grain size or suspended volume fraction.

The data collected along Transect 2 (Figure 4.3) shows that this mouth bar is currently in the progradational phase (Edmonds and Slingerland, 2007), which will end when the bar aggrades to the point that the momentum of the fluid upstream of the bar is unable to force water over the top of the bar, causing the flow to bifurcate and be diverted to the channels along the sides of the bar. The Edmonds and Slingerland (2007) model suggests that aggradation and bar progradation take place, to some extent, at the same time, and that aggradation becomes the dominant process again once the critical depth is reached. Our observations during the November deployment suggest two mechanisms that may dictate the rate of aggradation on the bar once the progradational phase has begun (see section 4.5).

4.3 ^{7}Be-dated short cores

Figure 4.4 shows the core locations and 90-day deposition amounts. The spatial pattern of deposition showns the highest rates of deposition arranged around the fringes of the mouth bar, which confirms the conclusion from the LISST/ADV transects that this bar is in a progradational phase. The only core on the main part of the mouth bar that shows zero deposition suggests the location of the divergence maximum discussed by Edmonds and
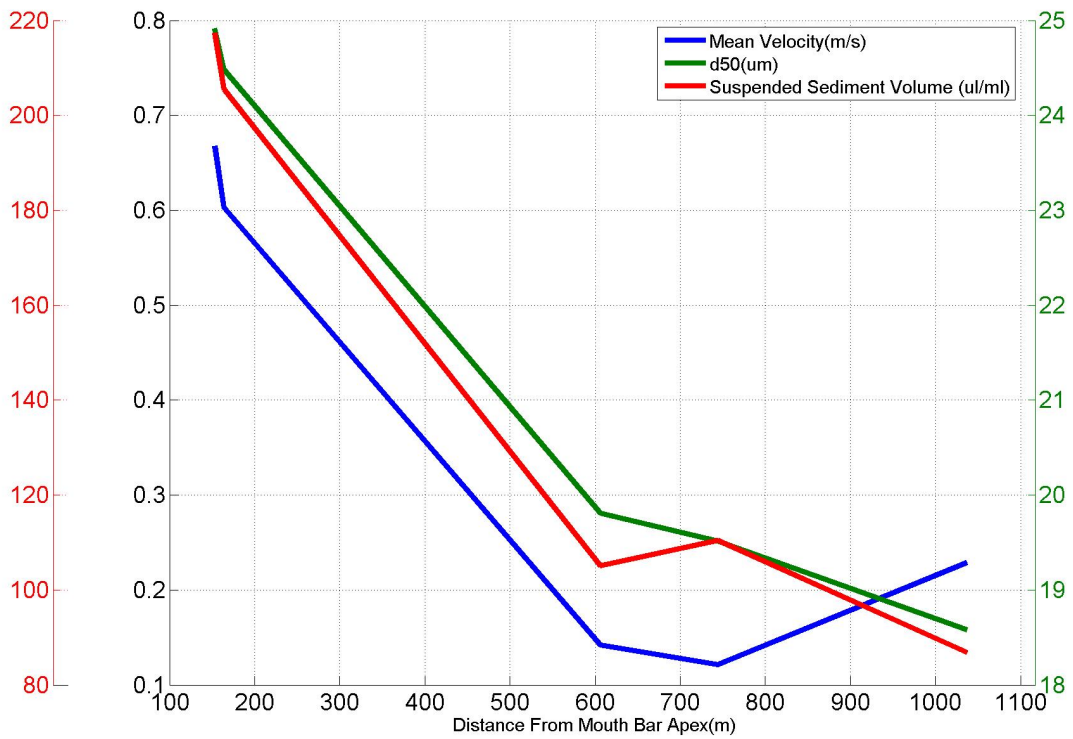
Figure 4.2: LISST/ADV Transect 1 shows data recorded from the bar apex to the distal end of the receiving basin during the April 2010 deployment. Velocity decreases along the transect, resulting in decreased suspended grain sizes and volumes. The small uptick in velocity seen in the last data point is due to flow constricting to exit the receiving basin, but the increase is not sufficient to remobilize sediments into the water column.
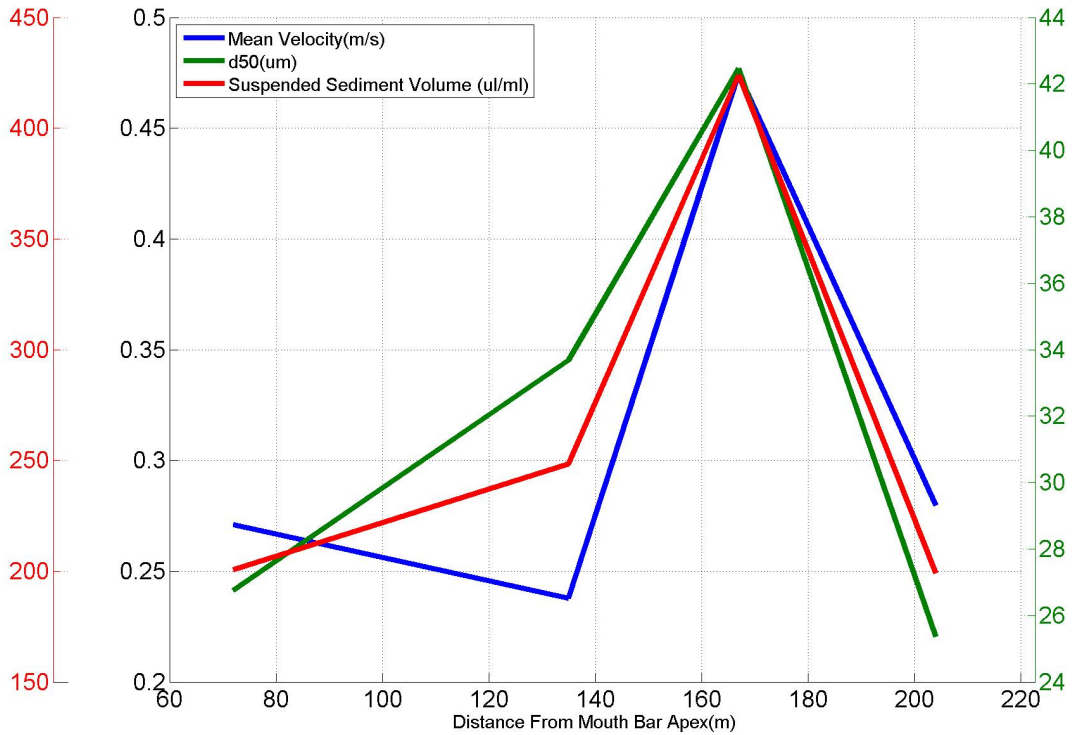
Figure 4.3: LISST/ADV Transect 2 shows data recorded from the apex of the mouth bar to its distal edge during the April 2010 deployment. Rising velocities are seen for the first 165 m, and falling velocities are seen beyond that. I attribute this pattern to the vertical constriction of flow on the bar top, as predicted by the conceptual mouth bar model. The increased velocities are able to scour the bar top sediments, resulting in more (by volume) and coarser sediments suspended in the water column, as seen in the median grain size and suspended sediment volume along the transect. These sediments are deposited at the distal edge of the bar, resulting in bar progradation.

Slingerland (2007).
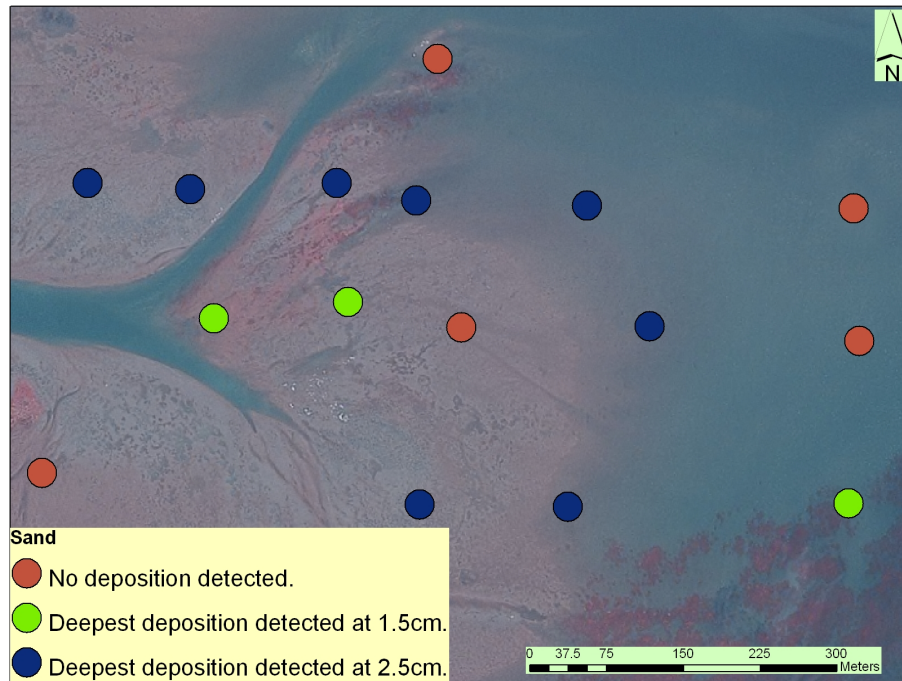
Figure 4.4: Mouth Bar Deposition: Deposition on the mouth bar is most intense around the fringes of the bar, indicating that the bar is in the progradational phase. Deposition of ^{7}Be was tested at 0.5, 1.5, and 2.5 cm below the surface. Blue dots indicate that deposition was detected at all three levels, and therefore 2.5 serves as a minimum depth of deposition. Green dots indicate that deposition was detected at the first two levels and brown dots indicate that no deposition was detected at any level. There were no sites where deposition was detected only at the first level.

4.4   Sediment Samples From Around The Splay

Figure 4.6 shows the median grain size diameters (d50s) from all bottom samples (includes grab samples and sampling done from the Be7-dated short cores) throughout the splay, and figure 4.5 shows all bottom samples with 10% sand content or higher (distributions with a d90 exceeding 63 μm). All data in this section are from the April 2010 flood.

We can see from Figure 4.5 that sand was commonly present in the feeder channels outside of the splay, as well as in all mouth bar samples that were analyzed for grain size (only 10 of the 16 short cores were analyzed for grain size), but was only occasionally present in the channels within the splay. The spatial intermittency of sand in the channel bed within the splay appears to indicate that all or nearly all of the sand is in suspension, or is in motion near the bed, for certain reaches, mirroring one of the central conclusions of Nittrouer et al. (2008)'s work on the transport of bed sediments in Mississippi River.

Sand was recorded at all locations on the mouth bar, but was only found in one of four samples taken in the receiving basin. [7]Be analysis of the remaining three cores found no evidence of any deposition at those sites during the 90 days prior to April 7, 2010. The basin sample showing sand is in an area that receives significant flow from the right channel bifurcating around the mouth bar. Interestingly, we note that a channel bottom sample taken in the left bifurcation channel did not show any sand present, indicating again that the sands are in suspension in the channels leading to the mouth bar. The median grain size (D50) plots (Figure 4.6) show essentially the same trend as the sand/no sand plots (Figure 4.5), but they highlight the variability of bed materials even within a single channel reach. The North and South forks of Brant's Pass (Channels 2.2 and 2.3) are particularly interesting in that the grain size in the bed increases significantly along the lengths of the channels.

4.5   November 2010 Field Data

A follow up expedition to the study site was conducted in November of 2010 during which time the Mississippi River carried significantly less flow than during the April expedition (Figure 3.1). Areas of the mouth bar that had been sandy and compacted significantly enough to walk on in April were covered in up to 20 cm of unconsolidated silt and mud in November, and were nearly inaccessible on foot. No live vegetation was observed on the
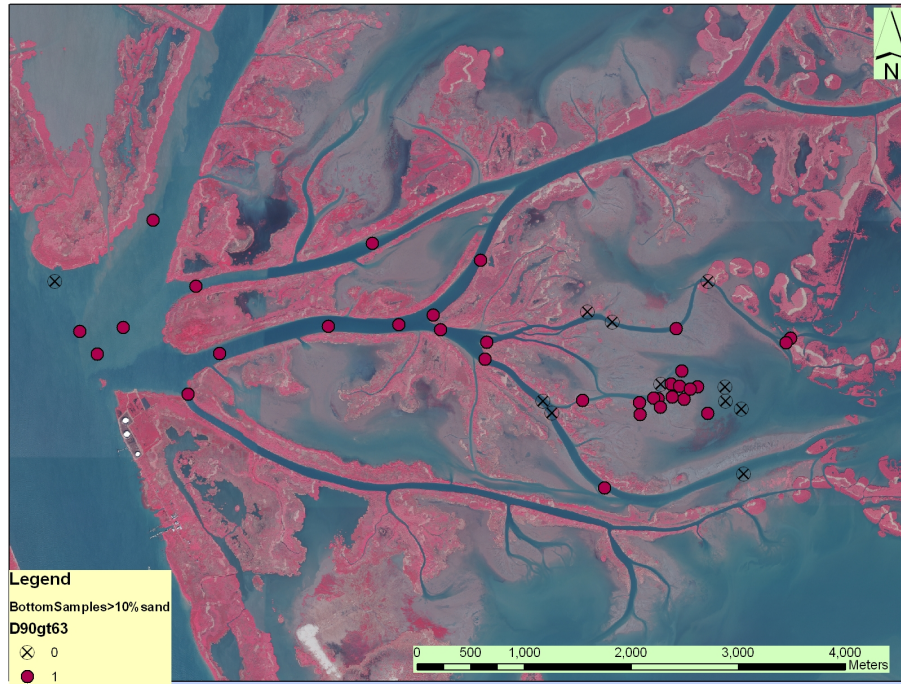
(a) Sand throughout the splay
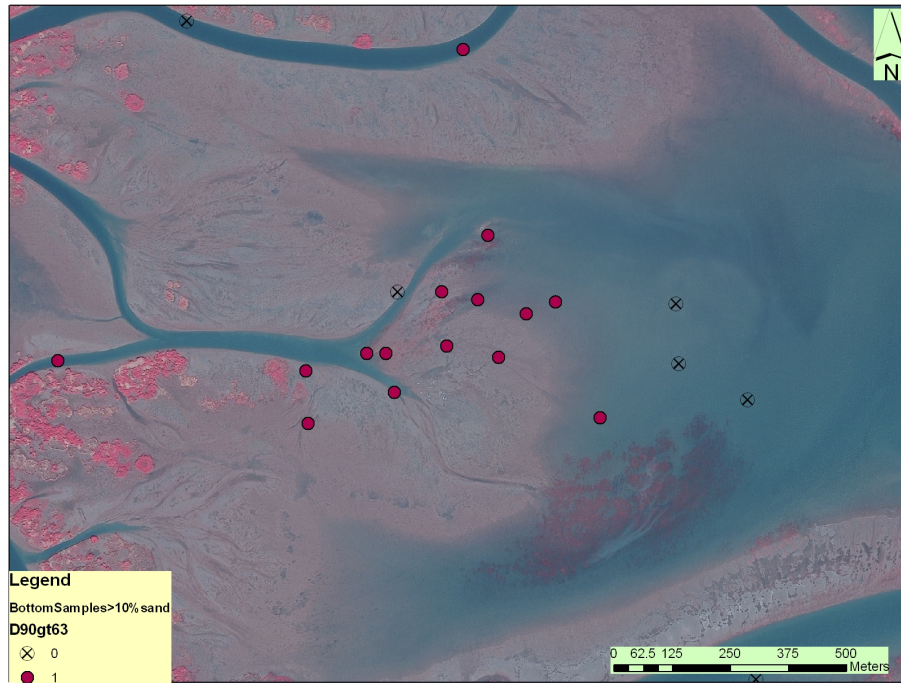
(b) Sand on the mouth bar.

Figure 4.5: Sand Distribution. Bottom samples with at least 10% sand are shown as filled circles.
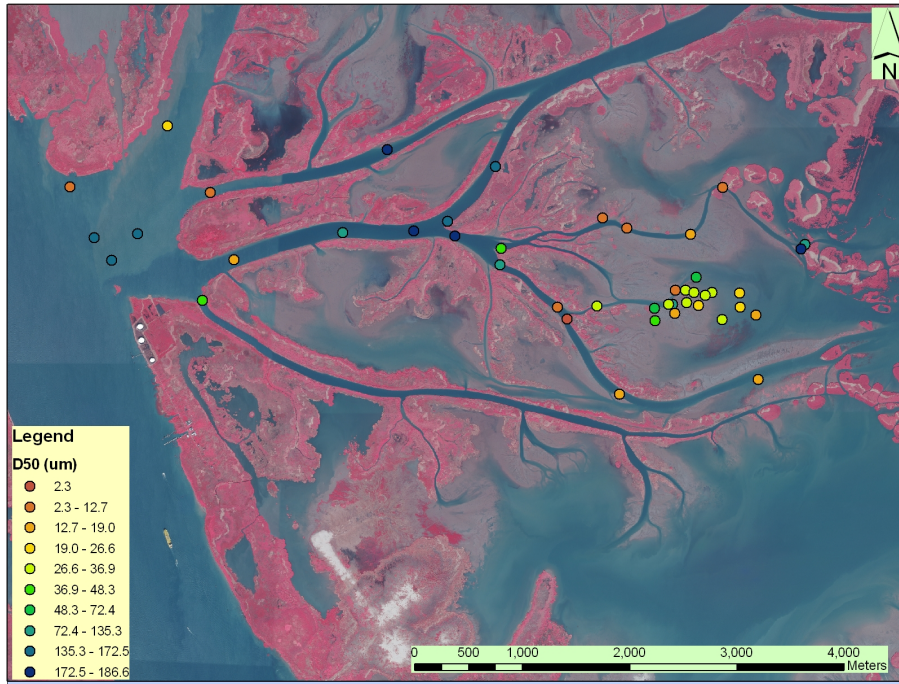
(a) Median Grain Size (D50) of bottom samples throughout the splay
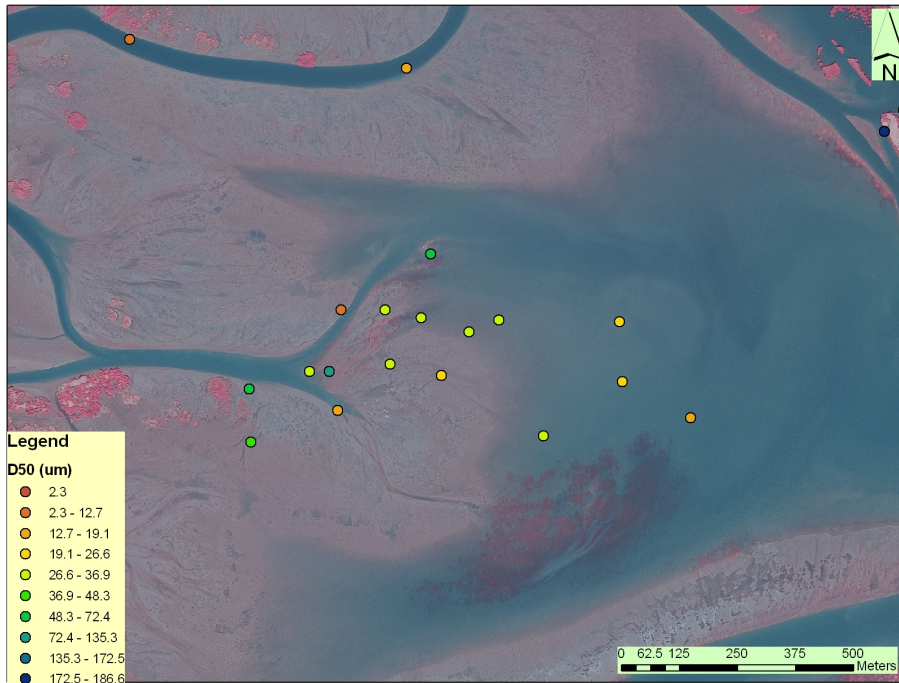
(b) Median Grain Size (D50) of bottom samples on the mouth bar

Figure 4.6: Grain Size Distribution

38

mouth bar during the April deployment except for scattered clumps of senesced S. deltarum. In November new clumps of S. deltarum had grown back and appeared to be thriving on the bar, and large mats of water hyacinth (Eichhornia crassipes) had been stranded on the bar top and in large quantities on the low spots surrounding the bar. These low spots had been part of the channel in April 2010, but were stranded when the water fell after the flood season.

One meter and half meter cores taken on the mouth bar in November show alternating layers of clay and sandier material. No pattern is evident in the thicknesses of the layers, though the contacts between different depositional regimes are often, though not always, abrupt. Core locations can be seen in figure 4.8, and core descriptions follow. Full core logs can be found in the Appendix.

4.6   Core Descriptions

MB-01. Core MB-01 was obtained on a mudflat near the apex of the mouth bar. The core was taken in two half meter sections using a Russian Peat Corer and extension tool. The top 34 cm is aqueous unconsolidated silts and clays that coarsen gradually into a sand layer by 34 cm. Below the 34 cm mark is a layer of moderately compacted sand that transitions abruptly back to silts and clays at 70 cm.

MB-02. Core MB-02 was obtained in a small runnel on the North edge of the mouth bar, approximately 2m from the water's edge. The entrance to the runnel was stranded above the water line and the runnel carried no flow. The core was taken in two half meter sections using a Russian Peat Corer and extension tool. The top 45 cm consist of aqueous unconsolidated silts and clays with small numbers of stray vegetation fibers throughout. Some thin (< 5 cm) bands of slightly sandier material are present below 28cm, and the core coarsens markedly after 45 cm into a sand layer that extends to

Figure 4.7: Mike Brown approaching core location MB-03 in November 2010. Beneath the layer of vegetation is a knee deep layer of mud and silt. In April 2010 this location on the edge of the channel was submerged, and no vegetation was present except for scattered tufts of senesced S. deltarum. Live S. Deltarum is seen on the higher ground in the background of this image.

92 cm before transitioning abruptly back into silt and clay. Several clayey clasts are present in the sand layer, but do not significantly alter the characteristics of the layer.

MB-02B. Core MB-02B was obtained in the same small runnel as MB-02, but approximately 15 cm from the edge of the main channel, in a patch of more stable, sandier surface material. The top layer is aqueous sandy clay that transitions to a sandier clay through an abrupt contact at 15 cm and then to a predominantly sandy layer through another abrupt contact at 28 cm. The sandy layer extends down to 92 cm. As with MB-02, the bottom contact is abrupt and some clay clasts are present in the sandy layer.

MB-03. Core MB-03 was obtained on a barren flat (sand, overlain by 2-3 inches of silt and clay) approximately 30m from the North edge of the mouth bar. In order to access the flat it was necessary to walk through approximately 25m of thick water hyacinth growing on top of knee deep mud and muck (see figure 4.7). The core was taken as a one meter section from a Russian Peat Corer. The upper several centimeters of the core are unconsolidated clay and silt, and an abrupt transition to a sandy layer occurs at approximately 4 cm. The rest of the core, down to 1m consists of alternating layers (2 - 12 cm thick) of clays and silts with sandier material. Contacts are typically abrupt, and there is no evident pattern in the thickness or distribution of the layers. The sandiest material is found between 33 and 38 cm, sandwiched between sandy clay above and clay below. The finest material is found between 55 and 72 cm, and is mostly clay with one slight increase in sand content between 55 and 60 cm down.

MB-04. MB-04 was obtained approximately 55 meters from the South edge of the mouth bar, but access to the core location could only be obtained on foot from a position further upstream because the channel as choked with water hyacinth, and therefore inaccessible by boat. The core was taken with a 1m Russian Peat Corer, but only one half meter of penetration could be obtained before the device was blocked by a sand layer. The top layer of the core is the now familiar aqueous, unconsolidated silt

and clay, and gradually transitions into a sand layer between 8 and 17 cm. At 17 cm the sand layer abruptly transitions into a clay layer that extends to 32 cm before coarsening to a sandy layer by 35 cm. Below 35 cm the core is mostly sand, with some thin layers of clayey material interspersed. As mentioned, the core could not penetrate below 50 cm, so presumably this sand layer extends below what is evident in the core.

MB-05. MB-05 was obtained on the left levee of the South main channel of the splay. It was not taken on the mouth bar. The top 10 cm of the core is missing, and was presumably aqueous material that leaked out during transportation. Below 10cm is aqueous clay that coarsens into a sand layer. Coarsening is complete by 28 cm and the sand layer extends to 37 cm, where it abruptly transitions back to clay material. Another sand layer is present between 50 and 56 cm, with sharp contacts to clay on the top and the bottom. Clay dominates below 56 cm, with an oxidized layer from 77 to 93 cm, suggesting organic material.

In order to fit these cores into the mouth bar analysis it is necessary to be certain that the cores are entirely composed of bar sediments. An analysis of water depths shows that the cores taken on the mouth bar are entirely bar sediments: The splay was formed as a result of a channel breaching its levee and flowing into the adjacent subsided basin. Depths exceeding 1.2 m were observed in the basin beyond the mouth bar and the maximum water depth observed over the mouth bar was 0.3m, so if we assume that this basin subsided uniformly then we can be confident that all but the lowest 10cm on the 1m cores represents the mouth bar. Removing the lowest 10 cm on all of these cores would not change this analysis at all, and the conceptual model presented above is still valid. Furthermore, there is no evidence in the cores of a peat layer that would indicate contact with a drowned marsh, so it is likely that even the bottom 10cm was deposited as a part of the splay and mouth bar processes. Thus, all of

the material contained in these cores, with the exception of MB-05, can be considered to be mouth bar material.
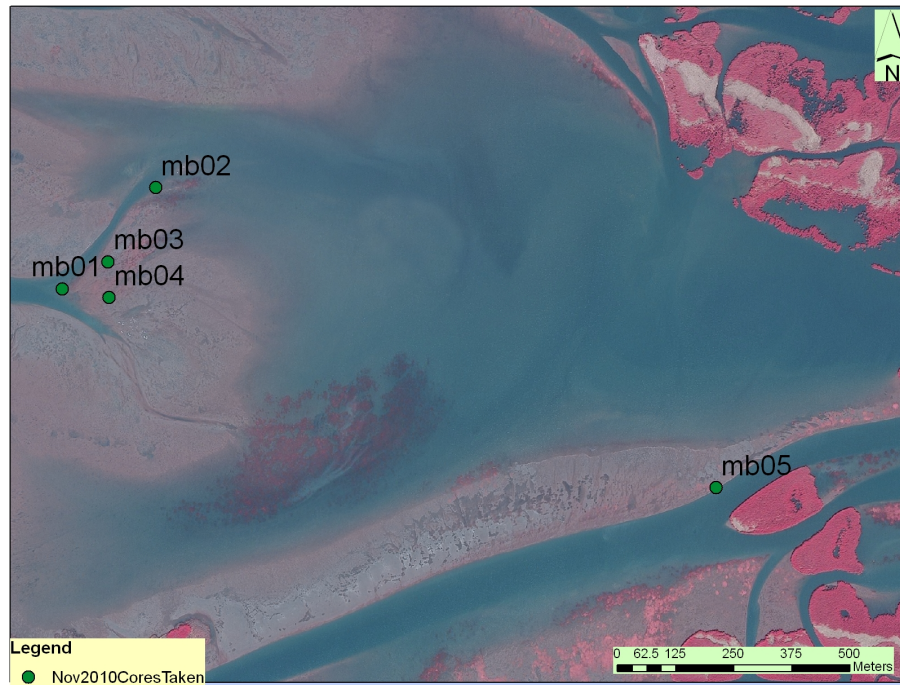
Figure 4.8: November 2010 Core Locations

4.7 Extended Model of Mouth Bar Deposition For River Dominated Wetland

It is clear from these cores that the conceptual model suggested by Edmonds and Slingerland (2007) does not fully explain the processes that led to the formation of this mouth bar. Instead of a three stage process of aggradation, progradation, and then runaway aggradation on the top of the mouth bar, we see evidence of cyclically changing depositional regimes that alternately deposit coarse and fine material in the same location. A striking feature of these cores is that a significant fraction (more than 50% in some cores) of the volume of sediment

that comprises the mouth bar appears to be finer material, suggesting that land building or processes that assist land building in this crevasse splay take place throughout a significant portion of the river year, rather than only during floods. Based on cores, observations, and hydrodynamic and sedimentary data collected in the field I suggest that the conceptual model for mouth bar deposition be extended to include flow conditions. I suggest three flow regimes, defined based on the presence or water over the mouth bar and the presence of sand in suspension in the channel feeding the mouth bar.

Flow Condition	Water Covers Bar	Sand In Suspension
High	Yes	Yes
Intermediate	Yes	No
Low	No	No

Table 4.3: The three flow regimes of the extended conceptual model

1. During periods of high flow the mouth bar might be in an aggradational, progradational or runaway aggradational phase. Sand can be transported as suspended load in the splay channels at higher river stages and then deposited on the bar, and potentially redistributed.

2. As the flood waters recede, the depth of water over the bar decreases, mimicking aggradation and driving the bar into a runaway aggradational phase during intermediate river stages. At intermediate river stages there is less - if any - sand suspended in the splay channels, and thus no sand will be deposited onto the bar. The water above the bar will contain only fine particles, which will be deposited on the bar as a cap over the sandy layer that was deposited at higher flows.

3. At low flows the bar is not covered by water, giving the newly deposited clays and silts an opportunity to dewater and consolidate. The consolidated fine sediments are

possibly able to resist the erosive force of the next spring flood, allowing the next sand layer to be deposited on top of a layer of fines.
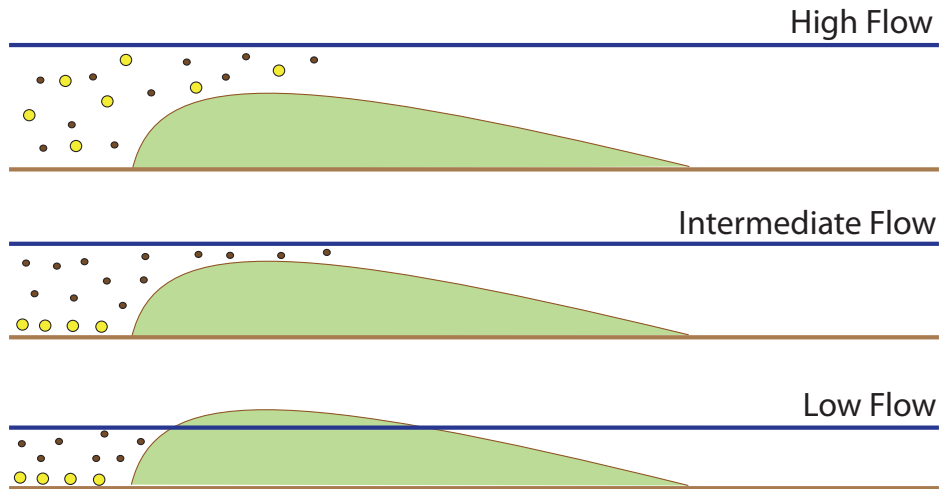
Figure 4.9: The three flow regimes of the extended conceptual model are defined by the presence or absence of water above the bar and of sand in suspension. Noncohesive material is indicated by the large yellow spheres, and cohesive material by the small brown spheres.

These three stages describe the bar at present but it is important to realize that the details and timing evolve as the mouth bar grows, therefore drawing conclusions about historical flow regimes based on the grain size of core material may not be a straightforward task. For example, the bar will eventually grow large enough to be in a runaway aggradational phase during high flows. When this occurs, the velocities on the bar will drop precipitously and make it unlikely that sand will be transported away from the channels to the interior of the bar in large quantities. The resulting deposition may be of finer particles, and could resemble the intermediate flow deposition described above. Or conversely, when the bar was in its early stages of development it is possible that intermediate flow conditions could have been sufficient to mobilize sand as bedload, resulting in a layer of sand that resembles what was earlier attributed to high flow conditions. The expanded conceptual model of deposition in this mouth bar is now described, but some critical questions about this system and this model remain.

1. What is the role of vegetation on the mouth bar?

   During the Spring 2010 flood, the bar was essentially barren except for widely spaced (5-10 m apart) patches of senesced S. deltarum, however by November S. deltarum was widespread on the bar, as were other rooted plants and large mats of water hyacinth that appear to have been washed onto the bar and stranded when the water receded. From these observations it would appear that the vegetation is washed away, drowned, or senescent during each flood season, but then grows back once the flood subsides. Because we cannot infer from this data set when the vegetation grew back it is impossible to speculate on how important it may be to the flow regime on the bar, or whether the vegetation plays a significant role in trapping particles during the intermediate flow stages.

   The root structures of the vegetation could play a role in stabilizing the bar during floods and preventing the layer of fine material from washing away, though it is impossible to determine the role of the roots without obtaining more comprehensive subsurface information. The cores examined here were taken selectively in barren areas of the bar, and as a result they contain few plant fibers and no evidence of the type of root network that would enhance soil stability.

   Field and laboratory experiments have shown that vegetation has the ability to significantly enhance sediment capture in marsh systems by reducing velocities, turbulent intensities, and vertical shear (Leonard and Reed, 2002; Nepf et al., 2005). The vegetative colonization patterns of this splay are already well documented (White, 1993); data collection with a goal of relating the timing of vegetative regrowth with flow into the splay, and relating local vegetation to the flow field and to sediment capture represent avenues along which this work could be significantly and readily advanced.

2. How prevalent are these processes? How does this mouth bar compare to typical river

mouth bars, like we might see in Southwest Pass or in the Wax Lake Delta?

Van Heerden and Roberts (1988) describe the distributary mouth sediments in the Atchafalaya Delta as an "overall coarsening-upward sequence of repeated upward-fining cycles of parallel and cross-laminated silts and fine sands that pass upward into parallel-laminated clays." While a comprehensive analysis of the core sediments in the present splay is not available, it does not appear that these cores present any sort of "overall coarsening-upward sequence," though silt-sand cycles are clearly evident in cores MB-03 and MB-04.

5

Model Methods

5.1 Description of Numerical Model, Delft3D

Delft3D is used herein to solve the two dimensional unsteady shallow water equations for incompressible flow on a single layer grid of varying thickness (a so-called σ-grid). The formulations used for fluid flow, suspended sediment transport, and exchange of sediment materials with the bed can be found below, however for a complete description of all aspects of the Delft3D suite, including the bedload transport the reader is referred to Lesser et al. (2004) or Deltares (2010a). A list of variable names can be seen in Table 5.1.

5.1.1 Governing Equations

The equations for conservation of horizontal momentum are

$$
\begin{aligned}
\frac{\partial U}{\partial t} &+ U\frac{\partial U}{\partial x} + \nu\frac{\partial U}{\partial y} + \frac{\omega}{h}\frac{\partial U}{\partial \sigma} + fV \\
&= -\frac{1}{\rho_0}P_x + F_x + M_x + \frac{1}{h^2}\frac{\partial}{\partial \sigma}\left(\nu_V\frac{\partial u}{\partial \sigma}\right)
\end{aligned} \tag{5.1}
$$

$$\frac{\partial V}{\partial t} + U\frac{\partial V}{\partial x} + V\frac{\partial V}{\partial y} + \frac{\omega}{h}\frac{\partial V}{\partial \sigma} - fU \tag{5.2}$$

$$= -\frac{1}{\rho_0}P_y + F_y + M_y + \frac{1}{h^2}\frac{\partial}{\partial \sigma}\left(\nu_V\frac{\partial u}{\partial \sigma}\right)$$

The depth averaged continuity equation in the absence of evaporation or precipitation is given by

$$\frac{\partial \zeta}{\partial t} + \frac{\partial \left(hU\right)}{\partial x} + \frac{\partial \left(hV\right)}{\partial y} = 0. \tag{5.3}$$

5.1.2   Suspended Sediment Transport

Suspended sediment transport is calculated with an advection-diffusion equation.

$$\frac{\partial (hc)}{\partial t} + \frac{\partial (hUc)}{\partial x} + \frac{\partial (hVc)}{\partial y} + \frac{\partial \omega c}{\partial \sigma} \tag{5.4}$$

$$= h\left[\frac{\partial}{\partial x}\left(D_H\frac{\partial c}{\partial x}\right) + \frac{\partial}{\partial y}\left(D_H\frac{\partial c}{\partial y}\right)\right]$$

$$+ \frac{1}{h}\frac{\partial}{\partial \sigma}\left[D_V\frac{\partial c}{\partial \sigma}\right] + hS$$

5.1.3   Suspended Sediment Exchange With the Bed

Erosion and deposition of non-cohesive sediments are modeled using the approach given by van Rijn (1993).

Erosion and deposition of cohesive sediments are turned on or off through the use of critical shear stresses for erosion and deposition (τ_{er} and τ_{dep}, respectively). Erosion can only take place when the bed shear, τ_o is greater than τ_{er}, and deposition can only take place when the bed shear is less than τ_{dep}.

Variable	Meaning
U, V	Generalized Lagrangian Mean velocity components $(\frac{m}{s})$
u, v, w	Eulerian velocity components in Cartesian coordinates $(\frac{m}{s})$
P_x, P_y	Horizontal pressure terms, approximated with the Boussinesq approximation (Pa)
M_x, M_y	Accelerations due to momentum sources or sinks $(\frac{m}{s^2})$
F_x, F_y	Accelerations due to horizontal Reynolds Stresses taken along σ-planes $(\frac{m}{s^2})$
h	Water depth (m)
t	Time (s)
f	Coriolis Parameter (s^{-1})
σ	Vertical coordinate in σ-units
ν_V	Kinematic Viscosity $(\frac{m^2}{s})$
ρ	Fluid density $(\frac{kg}{m^3})$
ζ	Water surface elevation (m)
c	Mass sediment concentration $(\frac{kg}{m^3})$
S	Sediment sources per unit area $(\frac{kg}{sm^2})$

Table 5.1: Model Variables

A base rate of erosion for cohesive sediments is specified in input, while the base rate of deposition is equal to the product of the sediment's fall velocity multiplied by its concentration in each sigma-layer. In both cases the rate used by the model to calculate bed fluxes is a function of the base rate, the bed shear stress, and the appropriate critical shear stress. A morphological acceleration factor is used to translate hydrodynamic timescales into morphological timescales as described by Lesser et al. (2004).

5.2   Model Bathymetry

In order to apply the numerical model to the splay system, it was necessary to generate a topographical surface representing the channels, the mouth bar, and their surroundings. A surface representing the channels was generated and inserted into a surface representing the areas outside the channels. The non-channel bathymetry will heretofore be referred to as the "marsh" bathymetry.

5.2.1 Channels

The channel bathymetry was derived from a bathymetry survey collected during the November deployment. A freely available ArcGIS based tool (Merwade, 2008) was used to interpolate the survey lines to a matrix of depths in the surveyed channels. The interpolating tool takes channel boundaries and center lines as input, both of which were digitized manually in ArcGIS. The resulting depth matrix was exported from ArcGIS and combined with the marsh bathymetry described below.

5.2.2 Marsh

The topographical surface outside of the surveyed channels was derived from the 2008 Louisiana DOQQ image, freely available online (Atlas, 2008). Depths in the splay, but outside of the channels, were surveyed during April 2010. The measurements were geolocated using a hand held Garmin GPS and the DOQQ pixel representing the location was identified using ArcGIS. The value of the infrared band at that pixel was extracted, and the infrared intensity was found to relate to depth using the regression equation shown in Figure 5.1. The infrared band was chosen because it showed more contrast compared to the other wavelengths.

Applying the regression model to the infrared intensity for the entire DOQQ image resulted in the marsh bathymetries shown in Figure 5.2. The surface generated by this method is a depth surface, which does not take the slope of the water surface into account. A West to East slope of 8×10^{-5}, which is in the range of water surface slopes observed in the splay during April 2010 (Table 4.2), was added to the surface to translate from depth to bathymetry.

5.2.3 Linking the Two Surfaces

The two bathymetry data sets were merged in Matlab, using the channel boundaries as boundaries between data sets. The channel bathymetry was surveyed to the vertical datum
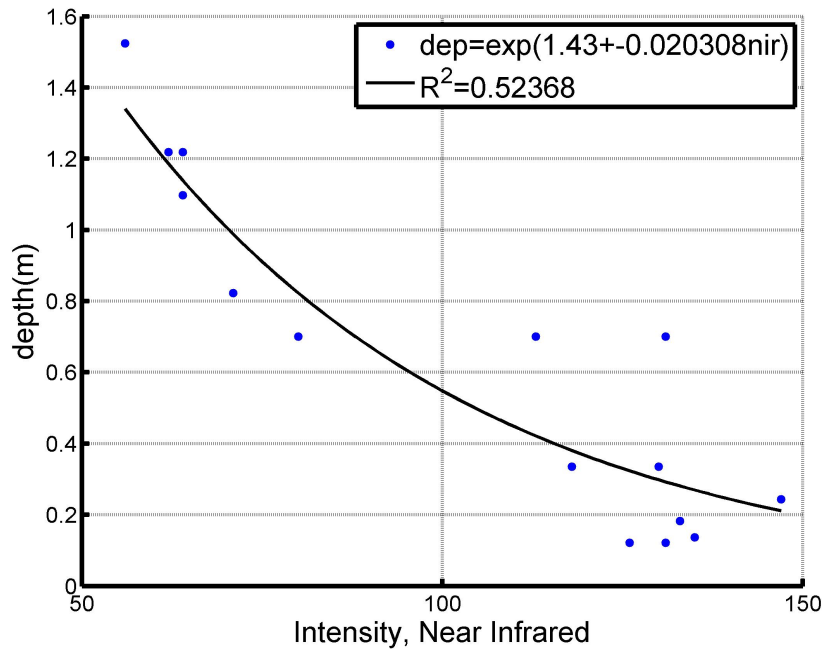
Figure 5.1: A least squares fit was used to determine the exponential relationship between measured depth and infrared intensity.

NAVD88, while the marsh bathymetry was not referenced to any vertical datum. In order to reference the marsh bathymetry to NAVD88, the vertical distance between the channel bottom and the bank at one location (Location 4.3, see 5.2) and was determined from the field data, and the marsh bathymetry was adjusted so that the vertical offset between the digitized channel bottom and bank matched the field data.

The final bathymetry surface was smoothed and interpolated to the model grid with Delft3D's bathymetry generating program, QUICKIN (Deltares, 2010b) (see Figure 5.3).

5.2.4 Computational grid

The model grid in the upper portions of the splay consists of 3m X 6m cells. Downstream of the mouth bar the grid transitions to 3m X 18m. The extra resolution in the upper splay was required to resolve the flow in channel reaches that intersect the grid faces at a diagonal. The grid y-resolution was chosen so that there were at least ten cells to represent the flow
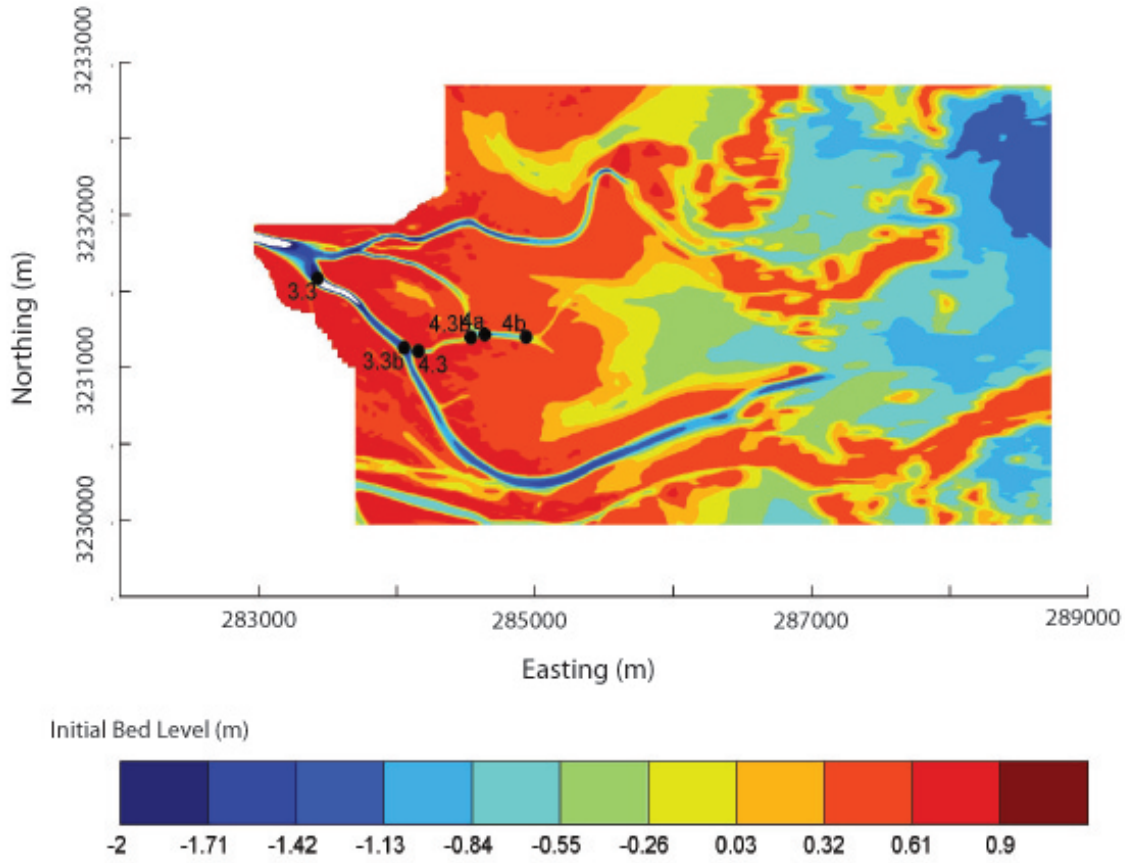
Figure 5.2: The initial topographic surface used with Delft3D. Vertical reference is NAVD88 in the final channel approaching the mouth bar.

5.3 Boundary Conditions

A constant flow boundary condition was applied to the upstream inlet. High flow scenarios were run with the observed April input of $260\frac{m^3}{s}$ and low flow scenarios were run with the observed November input of $40\frac{m^3}{s}$.

The downstream boundary condition was applied as a constant water level, the value
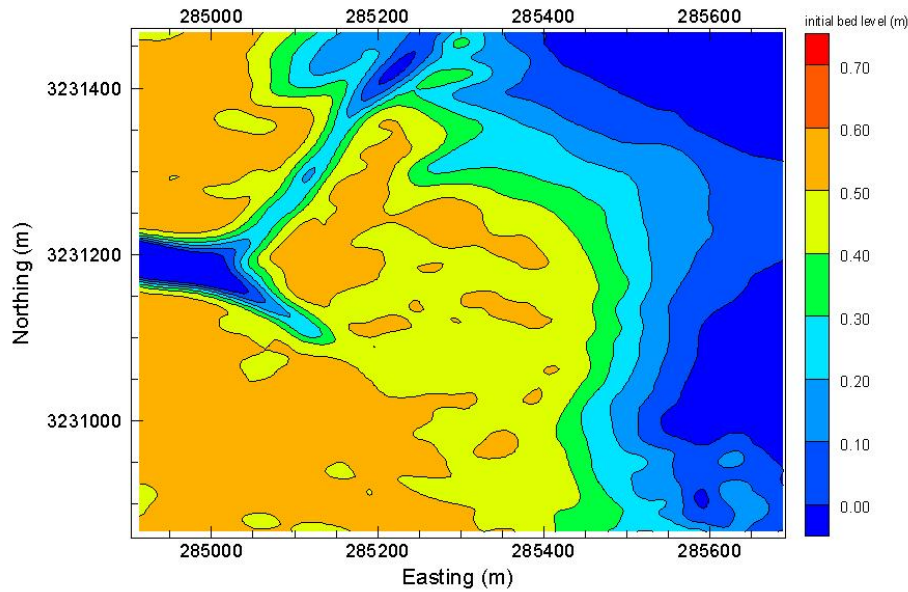
Figure 5.3: The initial topographic surface used with Delft3D, zoomed in on the mouth bar. Vertical reference is NAVD88

of which was computed in the following manner. The splay outlet is approximately 6 km from the Gulf of Mexico along the likely outflow path (as observed in satellite imagery), so assuming a water surface slope of 8×10^{-5} and a mean sea level of 0 m NAVD88 results in a mean water level of 48 cm NAVD88 at the outflow. Data collected in the downstream reach of the south channel showed a tidal range of approximately 20 cm during the April deployment. Thus a downstream water level in the range of 38 to 58 cm is an appropriate representation of the conditions observed in the field, though there is considerable uncertainty in this estimate. The hydrodynamic behavior of the model is validated with downstream controls of 40, 50, and 60 cm above NAVD88=0 m.

5.4   Hydrodynamic Validation

Before turning on the Morphology module it was necessary to verify that the numerical model captured the essential hydrodynamic characteristics of the natural system. Model

configurations were allowed to run for 12 simulation hours in order to reach steady state, at which point the water surface slope, the channel velocity, and the velocity and flow depth over the mouth bar were extracted and compared with field observations. Velocity magnitude in the water column just upstream of the bar apex was used to verify that the model has run to steady state. A typical example is seen in Figure 5.4. The results of the hydrodynamic validation can be seen in Table 5.2 and Figures 5.5 to 5.7. The most desirable combination of channel surface slope, bar depth and bar velocity was found with the model initialized to a 60 cm downstream control, which was used to initialize all model runs examined in Chapter 6.

5.4.1 Water Surface Slope

Surface slope was measured along two modeled reaches. Slopes for the upper splay were calculated between stations 3.3 and 3.3b and slopes for the lower splay were calculated between stations 4.3 and 4.3b. (See Figure 5.2) for station locations. The modeled slopes exceed the slope observed in the field, although efforts to correct the issue by lowering the bed friction coefficient resulted in undesirable flow oscillations.

Simulation	Upper Slope	Lower Slope
Downstream, 40cm	1.31×10^{-4}	1.14×10^{-4}
Downstream, 50cm	1.29×10^{-4}	1.14×10^{-4}
Downstream, 60cm	1.23×10^{-4}	1.10×10^{-4}

Table 5.2: Initialization water surface slopes after 12 simulated hours.

5.4.2 Mouth Bar Velocity and Depth

Simulated depths and velocity magnitude and direction are shown in Figures 5.5 through 5.7. The small number of samples on the bar surface limit the effectiveness of this validation step, and represents an improvement that can be made to this model in the future. For comparison with observations, desirable values of depth were near 70 cm in the basin beyond
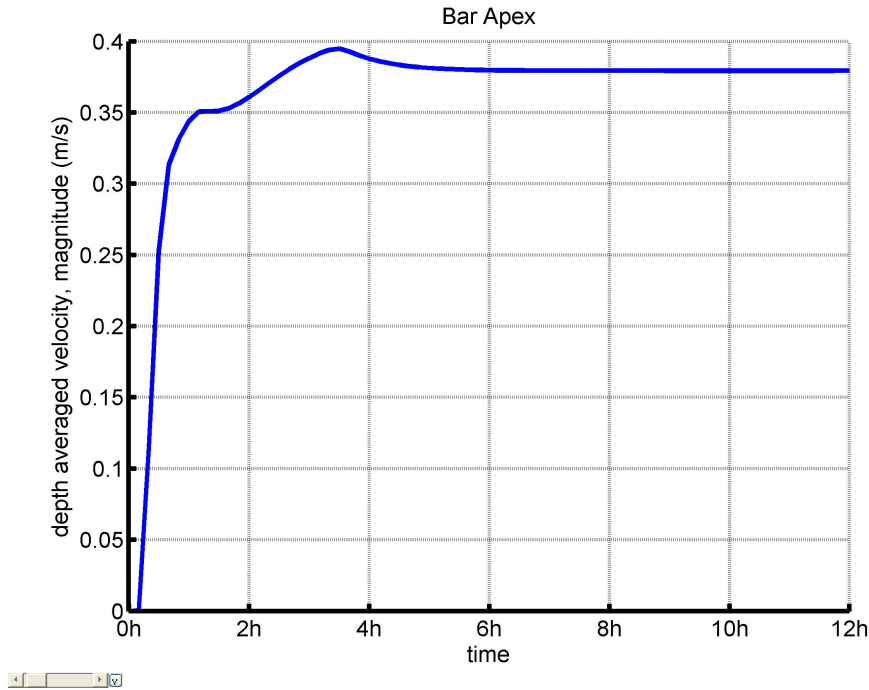
Figure 5.4: Velocity magnitude upstream of mouth bar, showing a typical covergance to steady state.

the distal edge of the mouth bar, and peak velocities near 45 cm/s in the preferential flow path. The model with the 60 cm downstream condition was chosen in spite of the low peak velocities on the bar, however these velocities appear once the morphology module is turned on and the flow is given time to scour a path.

5.5   Morphologic Validation

The morphology model is validated by comparison to the deposition data shown in Figure 4.4. Each model simulation shown in Figures 5.8 to 5.9 was run for an equivalent morphological time of 32 days. This number of days was chosen because it is the number of days between January 7, 2010 and April 7, 2010 that the Mississippi River met or exceeded it's flow during the field deployment on April 7 (see Figure 3.1). Assuming that [7]Be records deposition over the previous 90 days, and that the deposition observed on the bar took place during peak
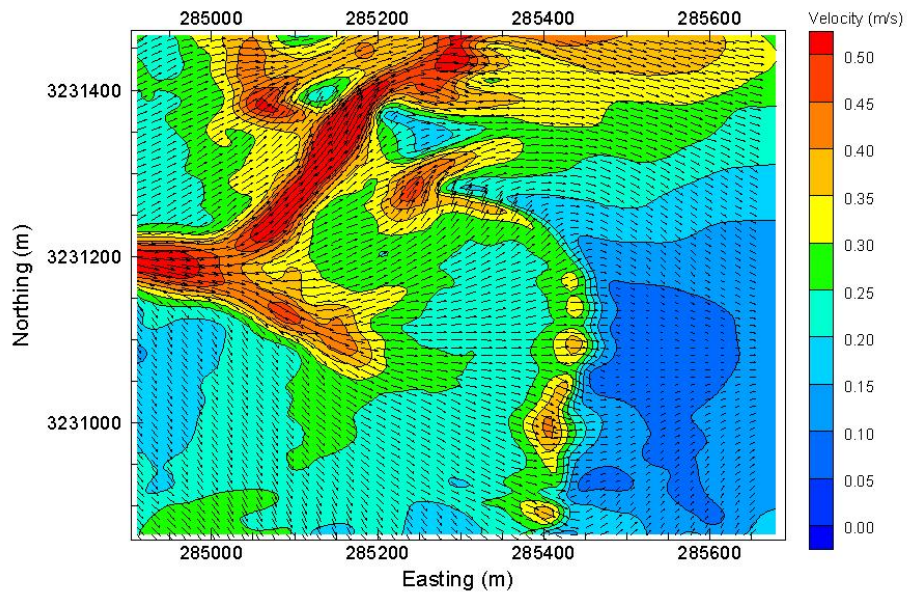
(a) Initialized Velocity. Bar top velocities between 21 and 49 cm/s along the preferential flow path on the north edge of the bar are in close agreement with those recorded in the field. See Figures 4.3 and 3.3 for the relavent field data.

Figure 5.5: Downstream 40 cm, Initialization
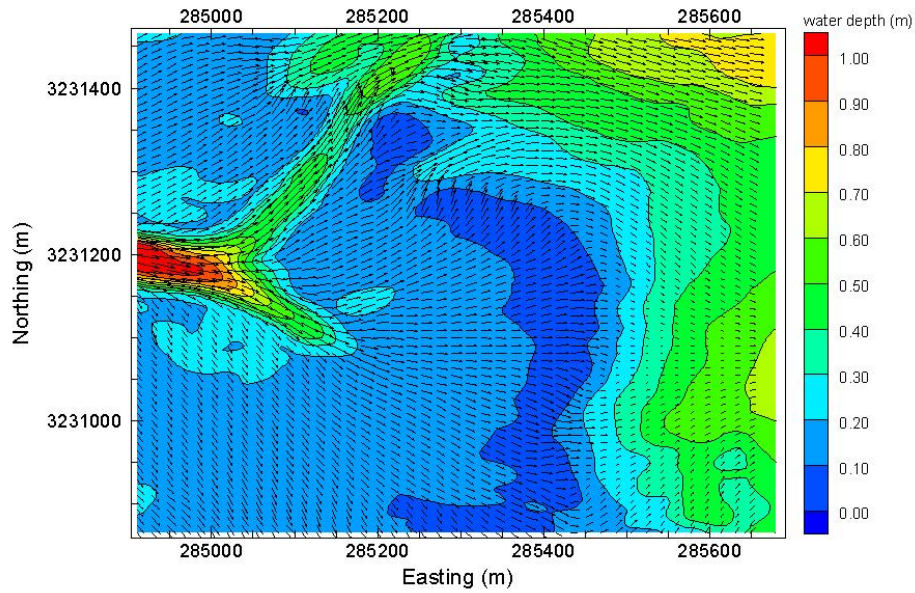
(b) Initialized Depth. The pattern of water depth over the bar matches the progradational phase of the conceptual mouth bar model described earlier. We see a band of vertically constricted flow (low depth) around the distal fringe of the mouth bar that matches with the band of increased velocity seen in above. That this reduction in depth is a result of a vertical constriction of flow rather than an increase in bed level can be confirmed by looking at the initial bed surface shown in Figure 5.3. Observations of depth along LISST/ADV Transect 2 (see Figure 3.3) were of depth between 24 and 34 cm, which is slightly deeper than the depth modeled here. Other field measurements showed depths of up to 70 cm along the distal edge of the bar, confirming that the model underestimates the depth of flow over the bar.

Figure 5.5: Downstream 40 cm, Initialization. (cont.)
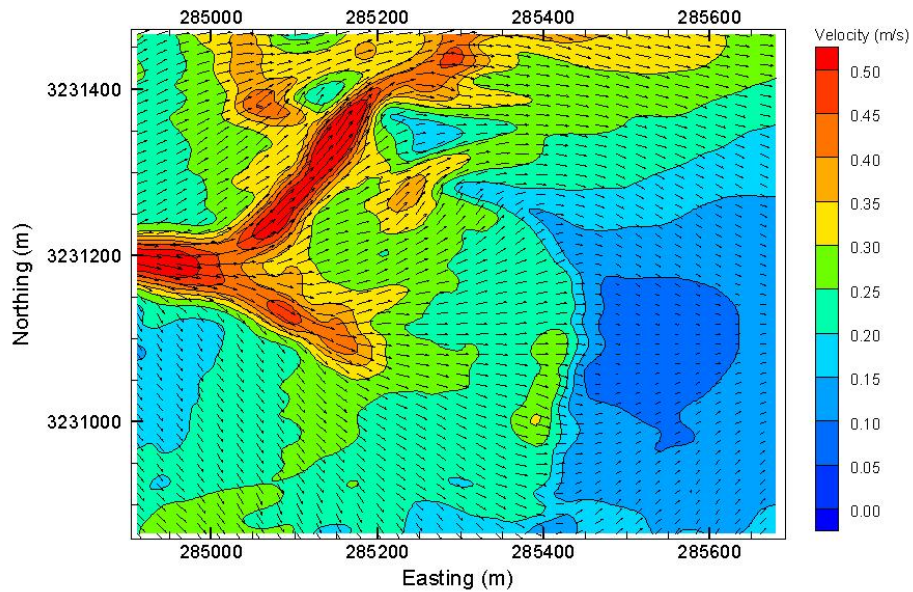
(a) Initialized Velocity. Peak velocities along the line of Transect 2 are in the 35 to 40 cm range, which is slightly lower than field observations. The high velocity fringe is still evident, though diminished, in some sections of the mouth bar.
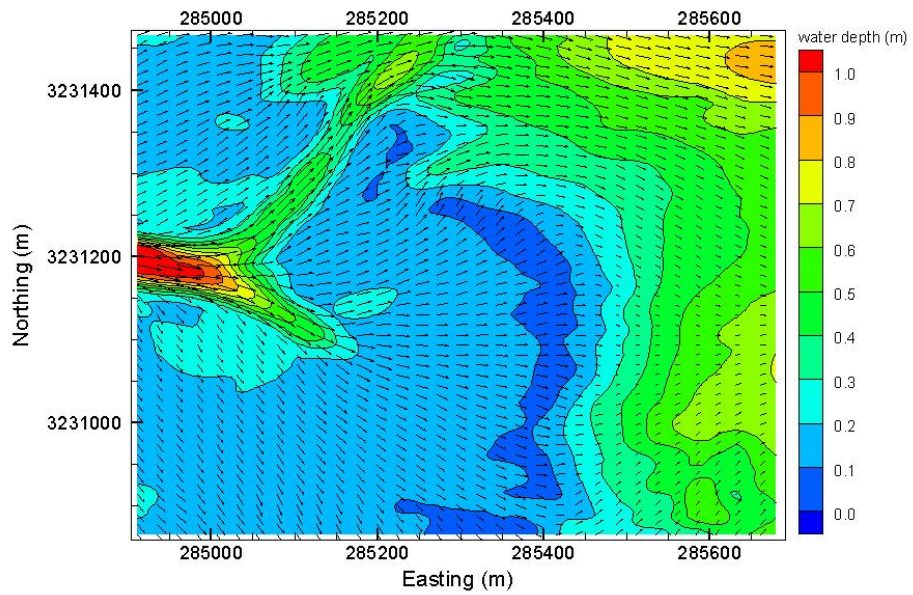
(b) Initialized Depth. Flow is again vertically constricted in a band. Depths along Transect 2 are in the range of observations.

Figure 5.6: Downstream 50 cm, Initialization.
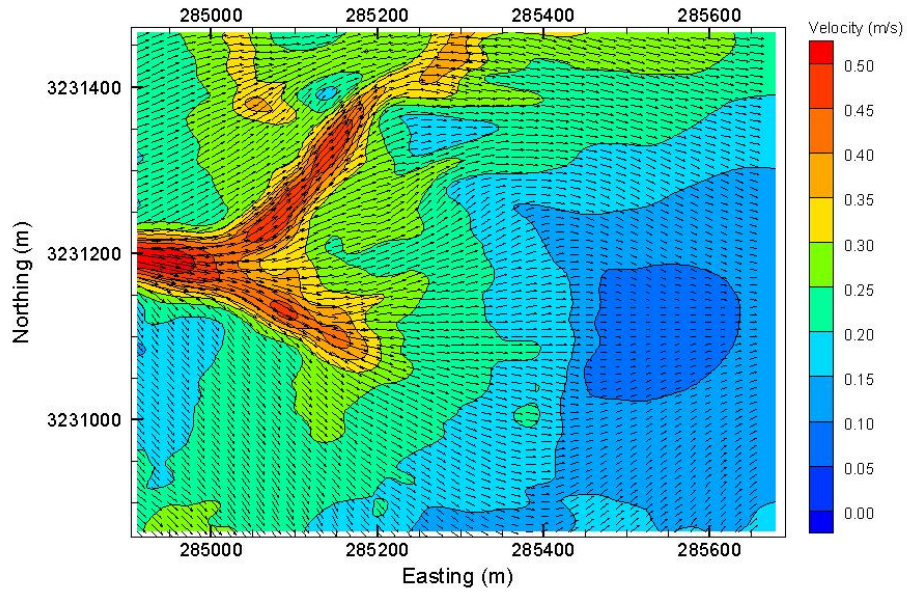
(a) Initialized Velocity. Velocities along Transect 2 are only half of those observed in the field.
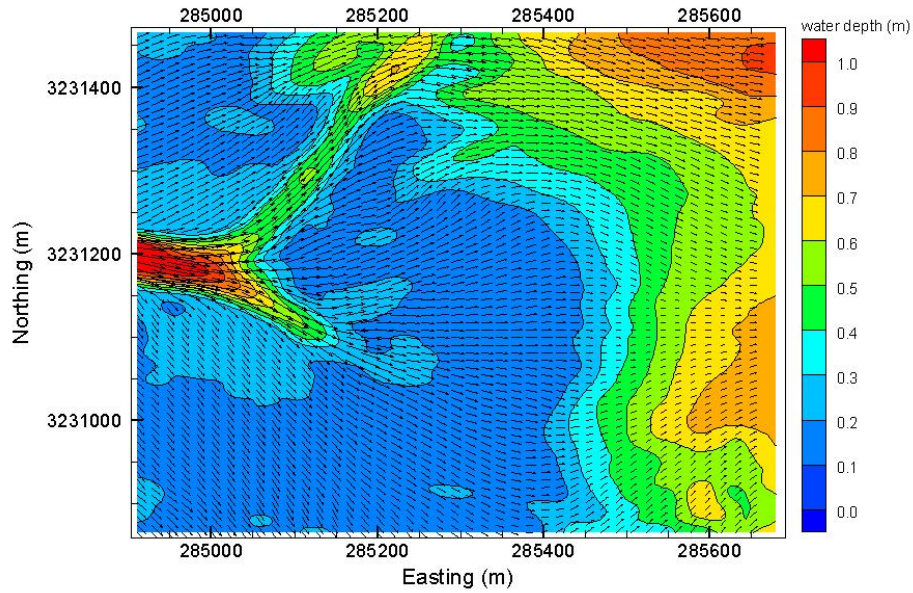
(b) Initialized Depth. Depths along Transect 2 are in the range of observations. The band of vertically constricted flow is no longer evident.

Figure 5.7: Downstream 60 cm, Initialization

river flows, then it is appropriate to determine the morphologically active time in this way, though the cutoff for peak flows is open to discussion.

Modeled results for a 32 day validation period are assessed on their ability to model the velocities in the preferential flow path and to model bar progradation. Models CGSplay52, CGSplay55 produce the most desirable results, and are examined in detail in Chapter 6. These two models will be run for an extra 32 days to observe the effects of continued fluvial and sediment input.

Model Number	CGSplay50	CGSplay52
TimeStep (min)	1	1
Upstream Flow (m^3/s)	260	260
Upstream Sediment Input, sand (μg/ml)	0.035	0.035
Upstream Sediment Input, cohesive (μg/ml)	0.15	0.15
Downstream (m NAVD88)	0.6	0.6
Manning's n	0.022	0.022
τ_{dep}, Cohesive	0.5	0.6
τ_{er}, Cohesive	0.4	0.35
Erosion Parameter, Cohesive	0.0001	0.0001
Cohesive Fall Velocity (mm/s)	1	0.25
Non Cohesive Mean Grain Size (μm)	150	150
MorphAc	30	30

Table 5.3: Simulation parameters for the runs analyzed in chapter 6
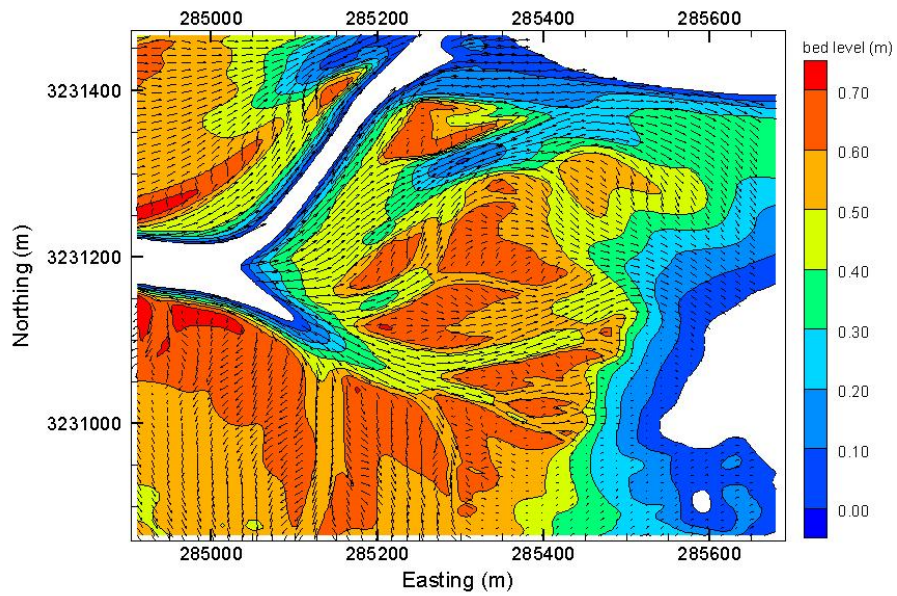
(a) A distinctly channeled surface has formed on the mouth bar. The preferential flow path towards the north edge of the bar is established and taking substantial flow. The right channel has scoured a path into the mouth bar, and bifurcated several times. Lunate bars mark the bifurcations. Significant deposition has occured to the north, near the outlet of the preferential flow path.

Figure 5.8: CGSplay50 after 32 days morphology.
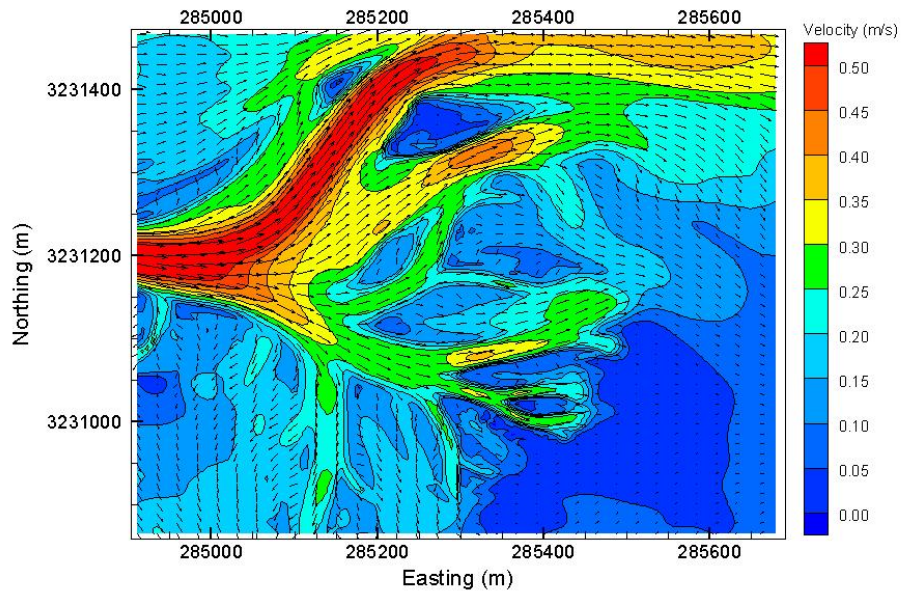
(b) Peak velocities on the bar are on the order of those seen in Figure 4.3

Figure 5.8: CGSplay50 after 32 days morphology. (cont.)
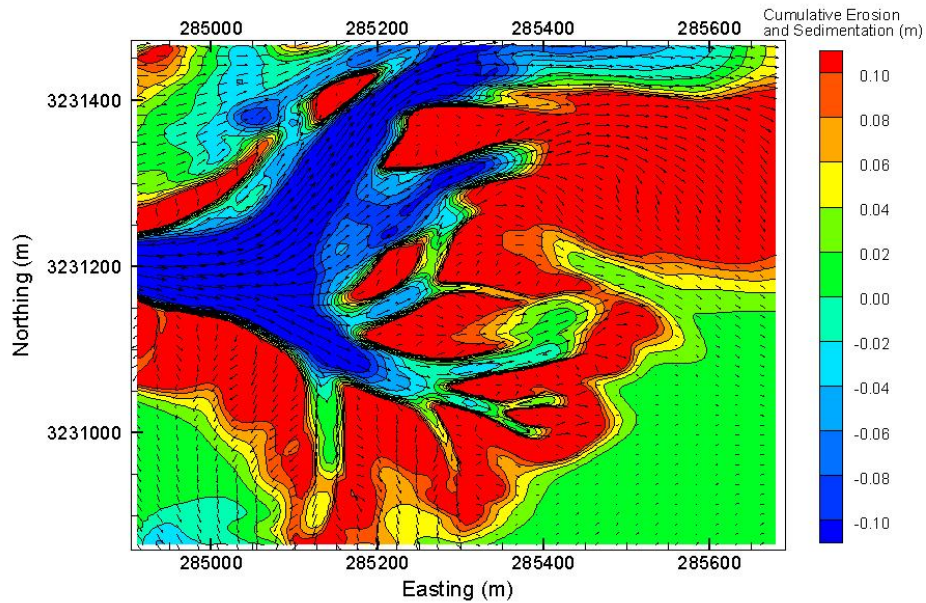
(c) Intense sedimentation is seen towards the distal edge of the bar. The bar apex has eroded significantly, which does not match the conceptual model, and satellite imagery showing that bifurcations tend to remain stable. The pattern seen in Figure 4.4, with moderate deposition near the bar apex, no deposition in the center of the bar, and intense deposition along the distal edge, is not in evidence here.

Figure 5.8: CGSplay50 after 32 days morphology. (cont.)
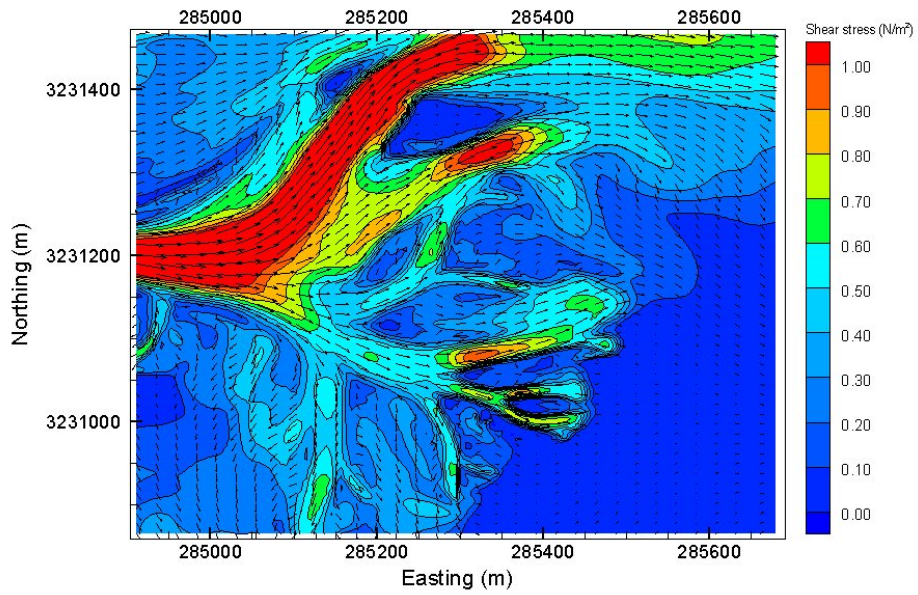
(d) Bed Shear distribution reflects the velocity distribution.

Figure 5.8: CGSplay50 after 32 days morphology. (cont.)
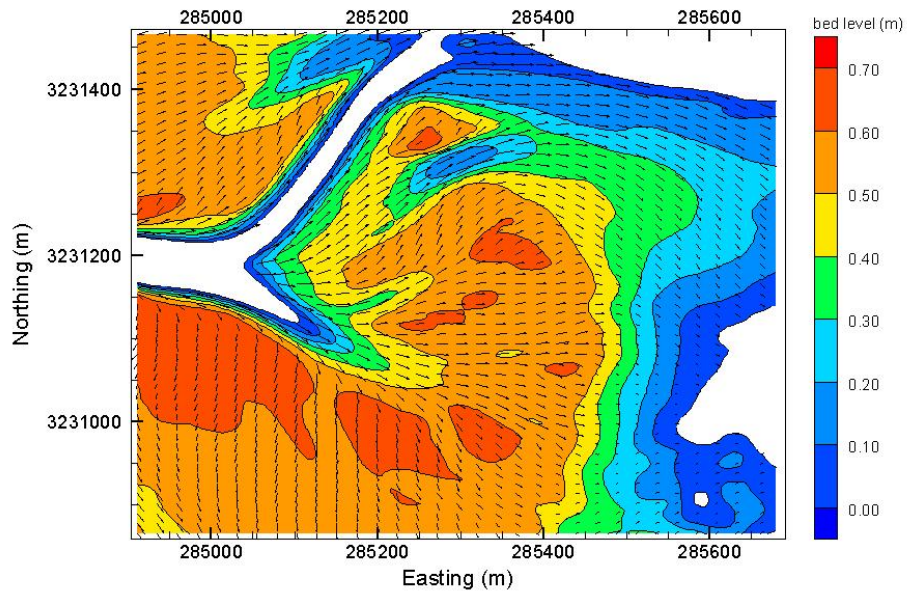
(a) The bar has clearly prograded into the basin. The bed level contours along the distal edge of the bar have prograded approsimately 50 m into the basin. Channelization is occuring, but not to the extent seen in CGSplay50.
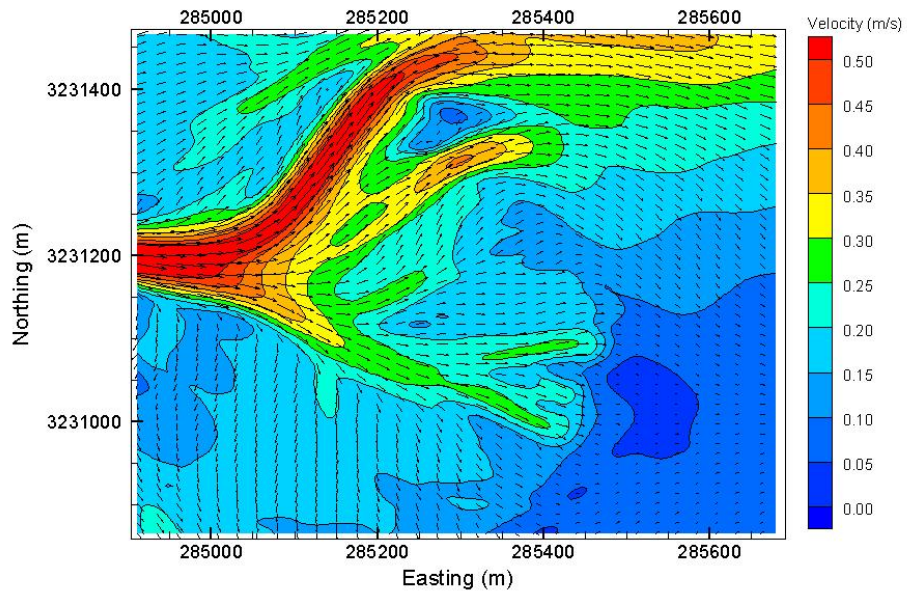
(b) The velocity distribution reflects a smoother surface than CGSplay50, with fewer channels. Peak velocities are above 0.4 m/s, matching field observations.

Figure 5.9: CGSplay52 after 32 days morphology.
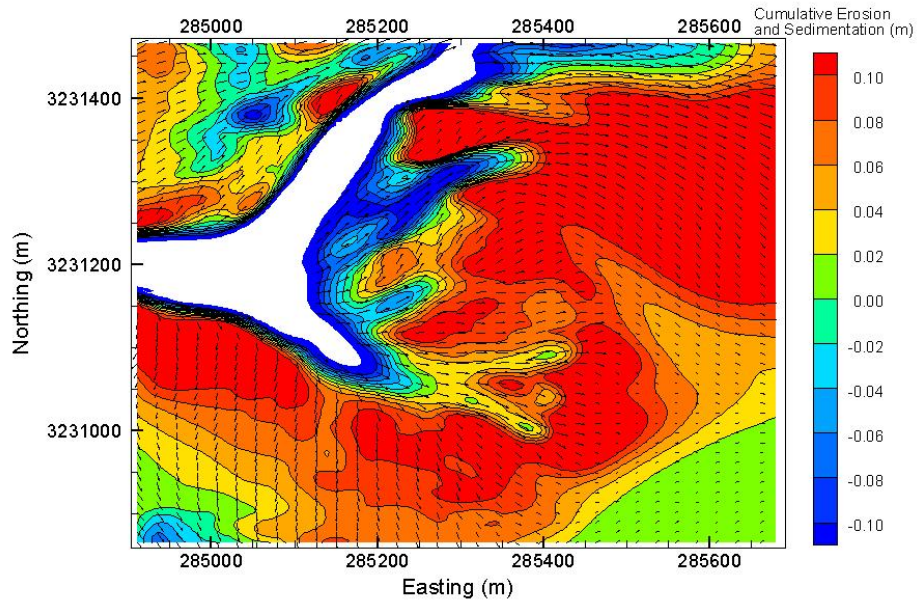
(c) Significant erosion has taken place at the bar apex. The pattern of deposition on the bar is confusing, but there is a clear band of intense deposition downstream from areas of more moderate deposition. While not matching theory or field observations exactly, the pattern of progradation can be seen.
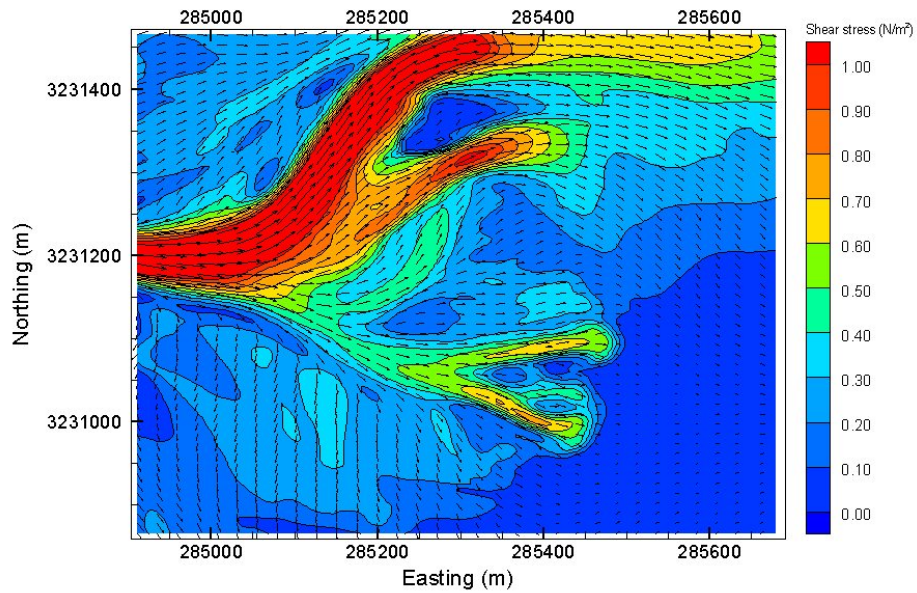
(d) Shear stresses match the velocity distribution.

Figure 5.9: CGSplay52 after 32 days morphology. (cont.)

6

Model Results and Discussion

6.1   Morphologic Experiments

The simulations selected after the validation procedures in Chapter 5 were run for an additional 32 days to observe the continued effects of fluvial and sediment inputs to the bar. The results were assessed to observe continued progradation or aggradation of the bar, and to observe the channelization of the bar surface. All three effects were observed, and the transition from progradation to runaway aggradation appears to be taking place in model CGSplay52. CGSplay50 shows a stabilization of the bar top channel network, evidenced by deeper channel incision and aggradation of the bifurcation mouth bars. The resulting bed surfaces and velocity fields can be seen in Figures 6.1 and 6.2.

6.2   Model Assesment

The models developed herein have been able to capture the essential characteristics of a prograding distributary mouth bar. Specifically, progradation at the distal bar edge is shown to occur at the expense of the surface further upstream, and the transition from progradation
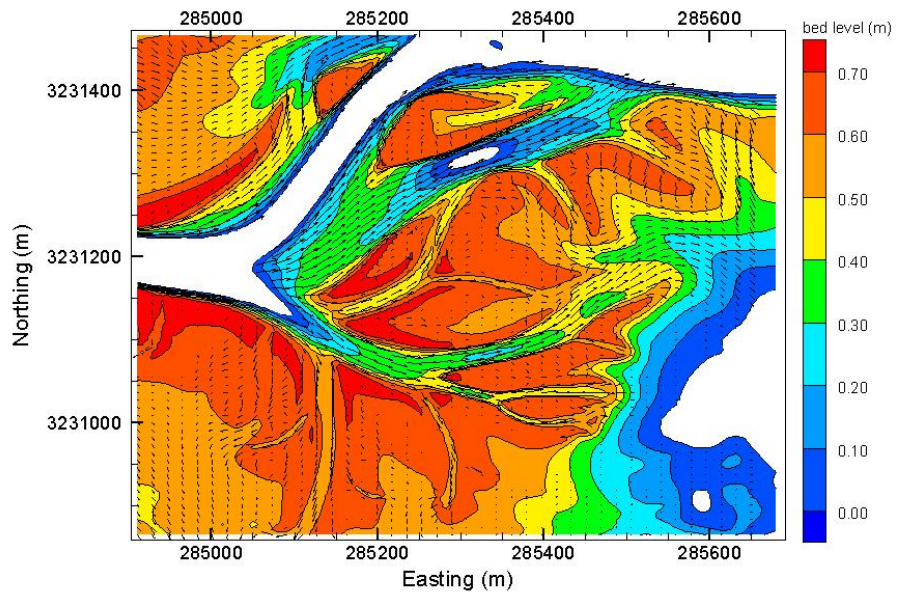
(a) CGSplay50 Bed Elevation (m) after 64 simulated days. Channelization of the bar top has deepened, and the bars marking the bifurcation points have stabilized and aggraded.

Figure 6.1: CGSplay 50
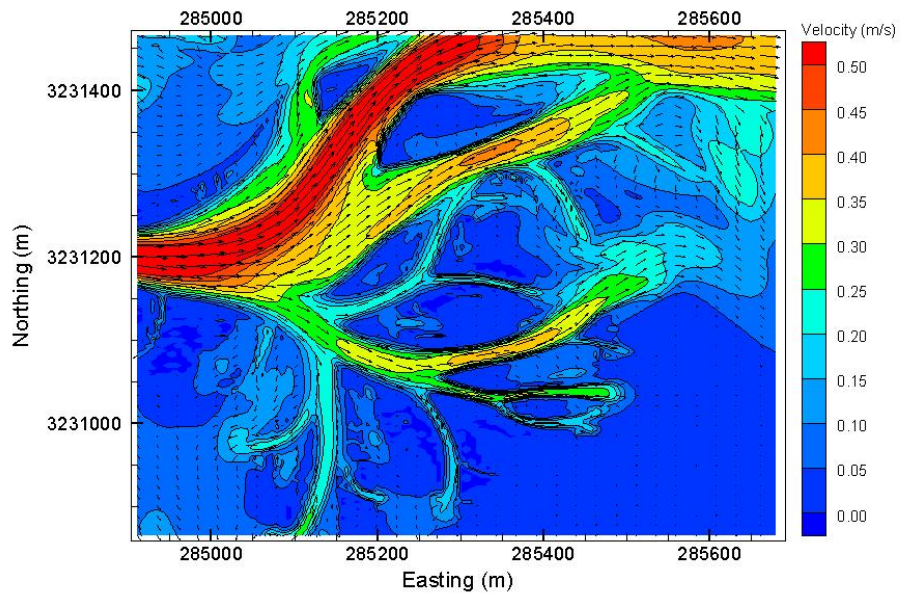
(b) CGSplay50 Depth Averaged Velocity (m/s) after 64 simulated days. The velocity field at 64 days is nearly indistinguishible from the field at 32 days, suggesting that some stable equilibrium has been reached.

Figure 6.1: CGSplay 50 (cont.)
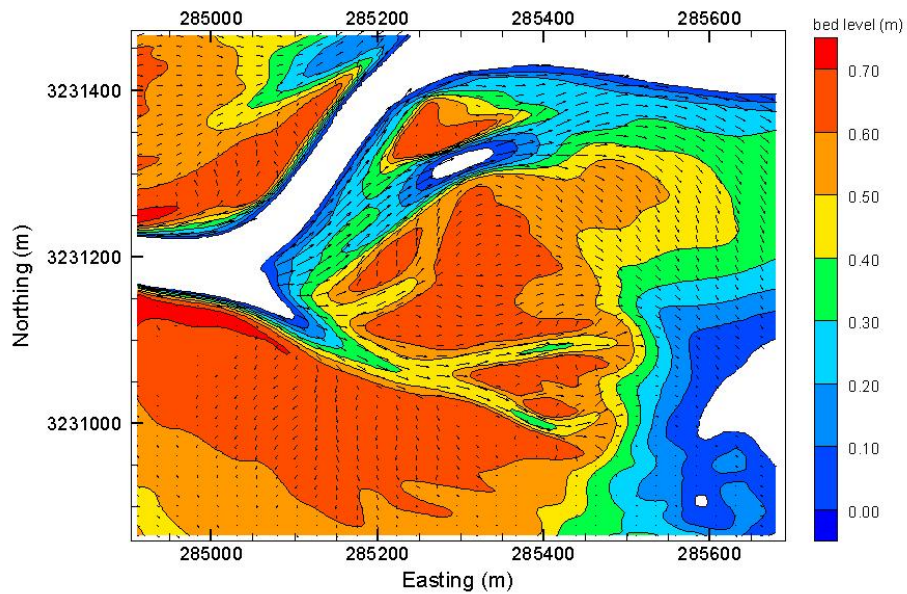
(a) CGSplay52 Bed Elevation (m) after 58 simulated days. Progradation continues at the distal edge of the bar. An aggradational feature on the bar top is beginning to have a significant effect on the flow field. The channels that were evident after the first 32 days have grown deeper and narrower. This image shows the result after 58 days, as the full 64 day simulation was available as of this writing.

Figure 6.2: CGSplay 52 after 58 days of simulation

71
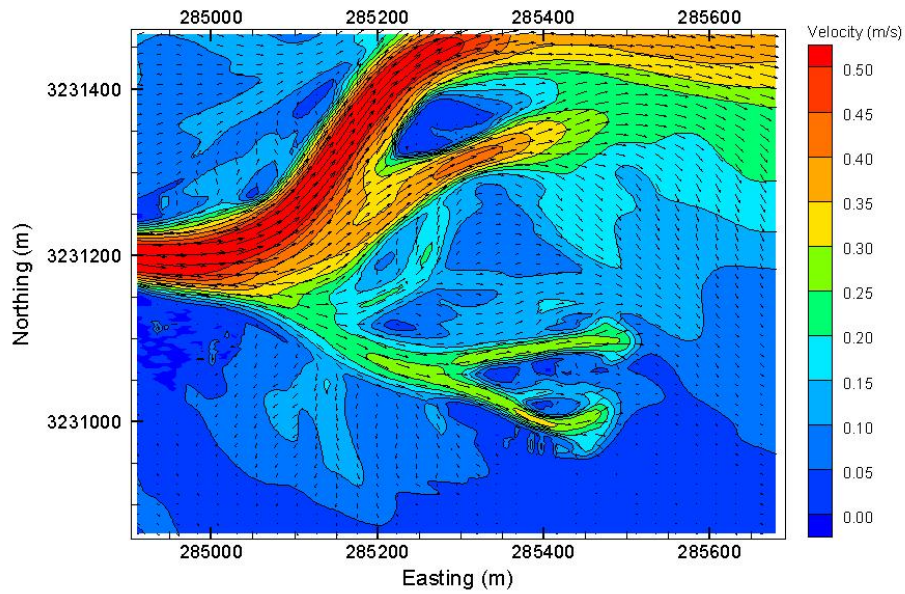
(b) CGSplay52 Depth Averaged Velocity (m/s) after 58 simulated days.. Velocities in the bar top channels have increased. The area of lower velocites in the center of the bar is a result of the aggradation seen in the bed surface, suggesting that the bar is transitioning into the runaway aggradation phase. This image shows the result after 58 days, as the full 64 day simulation was available as of this writing.

Figure 6.2: CGSplay 52 (cont.)

to runaway aggradation is evident. It would be incorrect to say that this model is a faithful representation of the hydrologic and morphologic behavior of the crevasse splay, or even of the small section of the crevasse splay -the mouthbar- that was examined in detail. However, the method of development and validation presented is able to produce a scenario that matches theory and field observations using minimal data inputs and a readily available tool (Delft3D). This suggests considerable room for improvement, but also that existing computational fluid dynamics techniques are advanced enough to competantly model scenarios outside of the main river channels.

The results also suggest several questions whose answers will add detail to the working conceptual mouth bar model.

1. To what extent are mouth bar surfaces channelized? The channelization observed in some model runs had significant consequences for the eventual morphology. It would be productive to study the surfaces of existing mouth bars in detail in order to determine whether flow is routed in chanels, and to what extent.

2. How do the morphological roles of cohesive and non cohesive sediments differ? Most of the morphological change seen on this bar is due to the transport of cohesive sediments. A useful experiment would be to alter the relative concentrations of the cohesive and non cohesive suspended sediment fractions and observe the resulting morphologies.

3. To what extent do progradation and aggradation overlap? Model results, particularly CGSplay52, show both processes to be simultaneous, though one or the other tends to dominate during a particular time period.

6.3 Uncertainty and Improvement

The initial topography used for the simulations discused herein represents a limitation for the model, and a potential area of improvement. An attempt to survey the bar was made during the November field deployment, but was postponed due to the unexpected and difficult surface conditions. More data points measuring depth in the receiving basin would improve the accuracy of the regression model used to transform NIR intensity into depth. Finally, a dataset showing the subaerial marsh elevation would help route flow more appropriately in the upstream channels. The state of Louisiana maintains a database of LIDAR topographies, but unfortunately the data does not extend below Venice.

Suspended sediment measurements throughout the water column and in the bed at the splay entrance would help characterize the sediment input condition. The sediment inputs used in these simulations were taken from research performed in the Mississippi River, and while a convincing case can be made to show that sediments in the upper parts of the water column in the river can be transported to and throughout the splay in suspension, it remains to be shown empirically. It is also likely that the grain size of non cohesive sediments in the splay is overestimated in the model. The mouth bar morphologies shown here are primarily the result of cohesive inputs. The sand fraction used to initialize the model was not transported by flow on to the bar in significant quantities, as was expected, thus virtually all of the morphological changes observed are the result of cohesive transport onto the bar, or re-entrainment of local bar sands.

Data on the vegetative growth in the splay exists (White, 1993), and could be compiled and related to flow conditions. Delft3D is able to model the effects of vegetation on fluvial flow, and field work compiling such data as the spacing and stem density of the bulrush clumps that were observed could improve the predictive capacity of the model and show convincingly the effects of vegetation on the conceptual mouth bar model.

7

Conclusions

Hydrodynamic and suspended sediment measurements collected on an actively growing distributary mouth bar show, and radionuclide dating of near surface sediments confirm, that the bar conforms to the progradational stage of the three stage mouth bar model advanced by Edmonds and Slingerland (2007). The conceptual model is extended on the basis of cores and field observations to account for seasonally varying riverine inputs. Three flow regimes are proposed, reflecting two criteria: 1) At high flows the bar is covered by water and sand is in suspension, resulting in a coarse deposit; 2) At intermediate flows the bar is covered by water but no sand is in suspension, resulting in a fine deposit; 3) At low flows the bar is exposed, allowing the fine deposit to consolidate and dewater. Significant deviations in the timing and intensity of the three stages are expected as the bar evolves over many seasonal cycles.

A methodology for developing a topographic surface in a marsh environment is presented, and the resulting surface is used to inform a numerical model that simulates the hydrodynamics and morphodynamics of a crevasse splay. The numerical model is able to capture the progradational phase of mouth bar development, and the transition into the runaway aggradational phase. A number of field data sets are suggested to improve the performance

of the model and the accuracy of the topographic surface. The model results suggest several improvements that can be made to the conceptual model, including studying the degree of channelization that is typical for mouth bars, and clarifying the respective morphological roles of cohesive and noncohesive sediments.

Studying systems of this type and scale can impact policy in South Louisiana. As regional administrators focus their efforts on planning multiple small to mid-sized diversions, it is important to have examples showing what the effects of such diversions can be. Most of our knowledge of deltaic deposition pertains to deposition at the mouths of rivers, where turbid buoyant plumes discharge into the open ocean, but from a management standpoint it is more appropriate to study deposition in shallow, protected, and less saline basins. The site considered herein is ideal for future study, particularly with respect to the effects of vegetation on mouth bar development and the ability of numerical models to effectively represent systems outside of the main river channel. It will also be important to find similar depositional systems in order to compare them with one another, and with the existing body of work on delta processes that occur at the river mouth.

Bibliography

Allison, M. (2009). Water and sediment surveys of the Mississippi River channel conducted at Myrtle Grove and Magnolia in support of numerical modeling (october 2008 - may 2009). Technical report, Louisiana Office of Coastal Protection and Restoration. 24 pp.

Allison, M. and E. Meselhe (2010). The use of large water and sediment diversions in the lower Mississippi River (Louisiana) for coastal restoration. *Journal of Hydrology 387*, 346–360.

Allison, M. A. (1998). Geologic framework and environmental status of the Ganges-Brahmaputra delta. *Journal of Coastal Research 14*, 823–836.

Allison, M. A., G. Kineke, E. Gordon, and M. Goni (2000). Development and reworking of a seasonal flood deposit on the inner continental shelf off the Atchafalaya River. *Continental Shelf Research 20(16)*, 2267–2294.

Atlas, L. (2008). Atlas: The Louisiana statewide GIS.

Babaeyan-Koopaei, K., D. Ervine, P. Carling, and Z. Cao (2002). Velocity and turbulence measurements for two overbank flow events in River Severn. *Journal of Hydraulic Engineering 128 No. 10*, 891–900.

Barras, J., J. Bernier, and R. Morton (2008). Land area change in coastal Louisiana - a multidecadal perspective(from 1956 to 2006).

Barras, J. A. (2006). Land area changes in coastal Louisiana after the 2005 hurricanes - a series of three maps. U.S. Geological Survey Open-File Report 06-1274.

Blum, M. D. and H. H. Roberts (2009). Drowning of the Mississippi delta due to insufficient sediment supply and global sea-levelrise. *Nature Geoscience 2*, 488–491.

Burdige, D. (2005). Burial of terrestrial organic matter in marine sediments: A re-assessment. *Global Biogeochemical Cycles 19*, 7pp.

Coleman, J. and S. Gagliano (1964). Cyclic sedimentation in the Mississippi River deltaic plain. *Transactions - Gulf Coast Association of Geological Societies 14*, 67–80.

Darby, F. and R. Turner (2008). Effects of eutrophication on salt marsh root and rhizone biomass accumulation. *Marine Ecology Progress Series 363*, 63–70.

Deltares (2010a). *Delft3D-FLOW User Manual* (Version 3.14, Revision 12556 ed.). Deltares.

Deltares (2010b). *Delft3D-QUICKEN User Manual* (Version 4.00, Revision 11003 ed.). Deltares.

Donnell, B. and J. Letter (1992). Two-dimensional modeling of alternative plans and impacts on the Atchafalaya bay and terrebonne marshes. Technical report, Army Engineer Waterways Experiment Station Hydraulics Lab. 118 pp.

Edmonds, D. A. and R. L. Slingerland (2007). Mechanics of river mouth bar formation: Implications for the morphodynamics of delta distributary networks. *J. Geophys. Res. 112*, 14.

Edmonds, D. A. and R. L. Slingerland (2009). Significant effect of sediment cohesion on deltamorphology. *Nature Geoscience 3*, 105–109.

Feng, H., J. Cochran, and D. Hirschberg (1999). ^{234}Th and ^{7}Be as tracers for the transport and dynamics of suspended particles in a partially mixed estuary. *Geochimica et Cosmochimica Acta 63*, 2487–2505.

Gagliano, S. M., J. M. Klaus, and K. M. Wicker (1981). Land loss in the Mississippi River deltaic plain. *GCAGS Transactions XXXI*, 295–300.

Galloway, W. (1975). *Process Framework for Describing the Morphology and Stratigraphic Evolution of Deltaic Depositional Systems*, pp. 87–98. Houston Geological Society.

Geleynse, N., J. E. A. Storms, M. J. F. Stive, H. R. A. Jagers, and D. J. R. Walstra (2010). Modeling of a mixed-load fluvio-deltaic system. *Geophys. Res. Lett. 37*, 7.

Geleynse, N., A. Storms Joep E., R. Walstra Dirk-Jan, A. Jagers H. R., B. Wang Zheng, and F. Stive Marcel J. (2011, Feb). Controls on river delta formation; insights from numerical modelling. *Earth and Planetary Science Letters 302*, 217–226.

Horowitz, A. (2010). A quarter century of declining suspended sediment fluxes in the Mississippi River and the effect of the 1993 flood. *Hydrological Processes 24*, 13–34.

Howes, N. C., D. M. FitzGerald, Z. J. Hughes, I. Y. Georgiou, M. A. Kulp, M. D. Miner, J. M. Smith, and J. A. Barras (2010). Hurricane-induced failure of low salinity wetlands. *Proc. Natl. Acad. Sci. U.S.A. 107*, 140–149.

Hoyal, D. C. and B. A. Sheets (2009). Morphodynamic evolution of experimental cohesive deltas. *J. Geophys. Res. 114*.

Kesel, R. H. (1988). The decline in the suspended load of the lower Mississippi River and its influence on adjacent wetlands. *Environ Geol Water Sci 11 No.3*, 271–281.

Kim, W., A. Dai, T. Muto, and G. Parker (2009). Delta progradation driven by an advancing sediment source: Coupled theory and experiment describing the evolution of elongated deltas. *Water Resources Research 45*.

Kim, W., D. Mohrig, R. Twilley, C. Paola, and G. Parker (2008). *Land Building in the Delta of the Mississippi River: Is it Feasible?*, Chapter 10, pp. 2–40. Final Report to Department of Natural Resources, Coastal Restoration Division, Baton Rouge, LA. Contract No. 2512-06-02.

LACPR (2007). Louisiana's comprehensive master plan for a sustainable coast.

Leonard, L. and D. Reed (2002). Hydrodynamics and sediment transport through tidal marsh canopies. *Journal of Coastal Research SI 36*, 459–469.

Lesser, G., J. Roelvink, J. van Kester, and G. Stelling (2004). Development and validation of a three-dimensional morphological model. *Coastal Engineering 51*, 883–915.

Mashriqui, H. (2003). *Hydrodynamic And Sediment Transport Modeling of Deltaic Sediment Processes*. Ph. D. thesis, Louisiana State University.

Meehl, G., T. Stocker, W. Collins, P. Friedlingstein, A. Gaye, J. Gregory, A. Kitoh, R. Knutti, J. Murphy, A. Noda, S. Raper, I. Watterson, A. Weaver, and Z.-C. Zhao (2007). *Global Climate Projections*. Cambridge University Press,.

Merwade, V. (2008). Creating river bathymetry mesh from cross-sections. Accessed March 31, 2011.

Morton, R., J. Bernier, J. Barras, and N. Fernia (2005). Rapid subsidence and historical wetland loss in the Mississippi delta plain: Likely causes and future implications. USGS open file report, United States Geological Survey. 128 pp.

Mueller, D. and C. Wagner (2009). Measuring discharge with accoustic doppler current profilers from a moving boat. U.S. Geological Survey Techniques and Methods 3A-22.

Nepf, H., B. Ghisalberti, and E. Murphy (2005). Mass transfer in vegetated shear flows. *Environmental Fluid Mechanics 5(6)*, 527–551.

Nittrouer, J. A., M. A. Allison, and R. Campanella (2008). Bedform transport rates for the lowermost Mississippi River. *J. Geophys. Res. 113*.

Nortek (2005). *Vector Current Meter User's Manual* (N300-100 - Rev. H ed.). Nortek.

Roberts, H. H. (1997). Dynamic changes of the Holocene Mississippi River delta plain: The delta cycle. *Journal of Coastal Research 13(3)*, 605–627.

Roberts, H. H. (1998). Early responses to the Atchafalaya to the Atchafalaya River diversion. *Journal of Coastal Research 14*, 882–899.

Saucier, R. (1994). Geomorphology and quaternary geologic history of the lower Mississippi valley. Waterways Experiment Station 2, U.S. Army Corps of Engineers. 363 pp.

Schleifstein, M. (2007). LSU researchers: coastal restoration projects doomed to fail. http://www.nola.com/news/index.ssf/2009/06/_timespicayune_projects_on_coa.html.

Sequoia (2007). *LISST-100X Particle Size Analyzer User's Manual* (Version 4.65 ed.). Sequoia.

Seybold, H. J., P. Molnar, H. M. Singer, J. S. Andrade Jr, H. J. Herrmann, and W. Kinzelbach (2009). Simulation of birdfoot delta formation with application to the Mississippi delta. *Journal of Geophysical Research 114*, 1.

Snedden, G. A., C. J.E., C. Swarzenski, and E. Swenson (2007, Jan). Sediment discharge into a subsiding Louisiana deltaic estuary through a Mississippi River diversion. *Estuarine, Coastal and Shelf Science 71*, 181–193.

Swarzenski, C. M., D. T.W., B. Fry, and H. T.G. (2008, Jan). Biogeochemical response of organic-rich freshwater marshes in the Louisiana delta plain to chronic river water influx. *Biogeochemistry 90*, 49–63.

Teledyne RD Instruments (2007). *WorkHorse Rio Grande ADCP Users Guide* (P/N 957-6167-00 ed.). Teledyne RD Instruments.

Tornqvist, T. E., S. J. Bick, K. van der Borg, and A. F. M. de Jong (2006, Aug). How stable is the Mississippi delta? *Geology 34*, 697.

Tye, R. and J. Coleman (1989). Evolution of Atchafalaya lacustrine deltas, south-central Louisiana. *Sedimentary Geology 65*, 95–112.

USGS (2005). West bay sediment diversion (mr-03) 2008 digital image map. USGS-NWRC 2005-02-0011.

USGS (2009). West bay sediment diversion (mr-03) 2008 digital image map. USGS-NWRC 2009-02-0315.

Van Heerden, I. L. and H. H. Roberts (1988). Facies development of Atchafalaya delta, Louisiana: A modern bayhead delta. *The American Association of Petroleum Geologists Bulletin 72*, 439–453.

van Rijn, L. (1993). *Principles of Sediment Transport in Rivers, Estuaries and Coastal Seas*. Aqua Publications. Amsterdam.

Welder, F. (1959). Processes of deltaic sedimentation in the lower Mississippi River. Technical report, Louisiana State University, Coastal Studies Institute, Baton Rouge, Louisiana. In: Technical Report No. 12.

Wellner, R., R. Beaubouef, J. Van Wagoner, H. Roberts, and S. Tao (2005). Jet-plume depositional bodies - the primary building blocks of wax lake delta. *Gulf Coast Association of Geological Societies Transactions 55*, 867–909.

Whipple, K. (2004). Surface process and landscape evolution notes. Chapter IV: Essentials of Sediment Transport.

White, D. (1993). Vascular plant community development on mudflats in the Mississippi River delta, Louisiana, USA. *Aquatic Botany 45*, 171–194.

Wright, L. and J. Coleman (1974). Mississippi River mouth processes: Effluent dynamics and morphological development. *Journal of Geology 82*, 751–778.

Yuill, B., D. Lavoie, and D. Reed (2009). Understanding subsidence processes in coastal Louisiana. *Journal of Coastal Research SI54*, 23–36.

Appendix A: Core Logs

UNIVERSITY OF NEW ORLEANS
COASTAL RESEARCH LABORATORY
VIBRACORE DESCRIPTION SHEET

CORE ID: _MB-01_   DATE: _11-15-10_   DESCRIBED BY: _myke b._

ELEVATION: _—_   LOCATION: _cubits gap_

CORE LENGTH: _1.0m_   COORDINATES: _-89.2108_   _29.1912_

TOTAL DEPTH: _1.0 m_   COMPACTION: _—_

SEDIMENTARY TEXTURE AND STRUCTURES	% SAND	PHYSICAL CHARAC-TERISTICS	STRATI-FICATION TYPE	SAMPLE	PHYSICAL DESCRIPTION:

PHYSICAL DESCRIPTION:

0.0 - 0.34m
clay, brown color, massive bedding. Aqueous in nature, unconsolidated. Bottom contact gradational.

0.34- 0.75m
sand, brown and black color, moderately consolidated. No shells, possible bio-turbation @ 0.74- 0.77 m. Bottom contact abrupt but gradational.

0.75- 1.0 m
Clay - trace SAND, brown clays, massive bedding. some bioturbation

Depth markers: 0.0m, 0.34m, 0.75m, 1.0m

Column notes: BROWN SANDS with some black oxidation

Figure A.1: Core MB-01

85

UNIVERSITY OF NEW ORLEANS
COASTAL RESEARCH LABORATORY
VIBRACORE DESCRIPTION SHEET

CORE ID: MB02

DATE: 15 NOV 2010

DESCRIBED BY: Chris E.

ELEVATION: —

LOCATION: Cubits (rap, Brant's splay)

CORE LENGTH: 1.0m

COORDINATES: -89.2088 / 29.1932

TOTAL DEPTH: 1.0m

COMPACTION: —

Legend:
- ⠇ sand
- ≡ clay
- Y organics

Core log columns: SEDIMENTARY TEXTURE AND STRUCTURES (CLAY, SILT, FINE SAND, MEDIUM SAND, COARSE SAND, GRAVEL, PEBBLE, INTERVAL (ft)); % SAND (0, 50, 100); PHYSICAL CHARACTERISTICS (COLOR, DEFORMATION, BED THICKNESS, % SHELLS, % ORGANIC, % BIOTURBATION); STRATIFICATION TYPE (WAVY, FLASER, LENTICULAR, CROSS BED, MASSIVE BED, INCLINED BED, HOR. LAMINAT.); SAMPLE (GRAIN SIZE, HEAVEY MINERAL, MICRO FOSSILS, RADIOMETRIC, RADIOGRAPH, PHOTOTGRAPH); PHYSICAL DESCRIPTION

Color annotations: br clay; black organics; brown sands

Depth markings: 0.0 m, 0.2, 0.45, 0.92, 1.0

PHYSICAL DESCRIPTION:

0.0-0.45 m
clay, brown, massive bedding
aqueous unconsolidated clay
stray vegetation fibers throughout,
though in small numbers.
thin bands of sand from
28 cm down. very black organic
material just above contact.

0.45-0.92 m
sand, brown or black,
massive bedding.
Uniformly fine sand for most
of section. several clayey
clasts (.7 & .82 m).
Abrupt transition to clay
between 0.91 & 0.92 m.

0.92-0.1 m
clay, brown or black.
massive bedding.
not fully consolidated, but
more consolidated than top
layer.

A note on color.
Core appears brown on outside,
but is blacker on the interior.
The contrast is more obvious
with sand layers but is true
for clay as well.

Figure A.2: Core MB-02

CORE ID: _MB-02B_   DATE: _11-15-10_   DESCRIBED BY: _myke b_
ELEVATION: _—_   LOCATION: _cubits gap   eastern grid   6" from waters_
CORE LENGTH: _1.0 m_   COORDINATES: _-89.2088   29.1932_   _edge_
TOTAL DEPTH: _1.0 m_   COMPACTION: _—_

SEDIMENTARY TEXTURE AND STRUCTURES	% SAND	PHYSICAL CHARACTERISTICS	STRATIFICATION TYPE	SAMPLE	PHYSICAL DESCRIPTION:

PHYSICAL DESCRIPTION:

0.0 - 0.15 m
clay-SAND, brown color, massive bedding. s. unit is aqueous & unconsolidated clay and fine grain sand. Bottom contact is gradational, it fines upward.

0.15 - 0.28 m
clay-SAND, brown color, massive bedding. Bottom contact sharp.

0.28 - 0.92 m
sand-clay, brown color with black sploches of trace organics. Bedding is not apparent, massive, shell fragment @ 0.55 m aprox. 2 mm in length. A clay clast is present @ 0.84m 3 cm in size. Bottom contact sharp, Root trace @ 0.34m

0.92 - 1.0 m
clay, brown with black splotches, no apparent bedding

Figure A.3: Core MB-02B

UNIVERSITY OF NEW ORLEANS
COASTAL RESEARCH LABORATORY
VIBRACORE DESCRIPTION SHEET

CORE ID: __MB03__   DATE: __15NOV2010__   DESCRIBED BY: __Chris Esposito__

ELEVATION: _____   LOCATION: __Cubits Gap, Brant's Splay__

CORE LENGTH: __1.0 m__   COORDINATES: __89.2098 / 29.1918__

TOTAL DEPTH: __1.0 m__   COMPACTION: _____

SEDIMENTARY TEXTURE AND STRUCTURES								% SAND			PHYSICAL CHARAC-TERISTICS					STRATI-FICATION TYPE						SAMPLE					PHYSICAL DESCRIPTION:
CLAY	SILT	FINE SAND	MEDIUM SAND	COARSE SAND	GRAVEL	PEBBLE	INTERVAL (ft)	0	50	100	COLOR	DEFORMATION	BED THICKNESS	% SILT	% ORGANIC	% BIOTURBATION	WAVY	FLASER	LENTICULAR	CROSS BED	MASSIVE BED	INCLINED BED	HOR. LAMINAT.	GRAIN SIZE	HEAVEY MINERAL	MICRO FOSSILS	RADIOMETRIC	RADIOGRAPH	PHOTOTGRAPH	

:: sand
= clay

0.0-0.04m
clay, brown, massive
Abrupt transition to coarser
material at 0.04 m

0.04 – 0.33 m
sand-clay, brown
bedding not apparent
Layers of sandier material
alternate with clayey material.
Abrupt transition from a
clay layer to a strongly
sand layer at 0.33 m

0.33 m – 0.38 m
sand, brown, massive
seems sandier @ top of layer.
This is the purest sand in
this core.
Grains have transitioned to
pure clay by 0.4 cm

0.38 – 0.72 m
clay-sand, brown
bedding not apparent
Layers of sand appear in this
otherwise clayey section

0.72 – 1.0 m
sand-clay, brown
bedding not apparent
sand is dominant in this
layer, with some intervals of
clayer material

color: brown or grey/black

Figure A.4: Core MB-03

UNIVERSITY OF NEW ORLEANS
COASTAL RESEARCH LABORATORY
VIBRACORE DESCRIPTION SHEET

CORE ID: MB04 DATE: 15 NOV 2010 DESCRIBED BY: Chris Esposito
ELEVATION: — LOCATION: Cubit's Gap, Brant's Splay
CORE LENGTH: 0.5m COORDINATES: -891.2098' 29.1911
TOTAL DEPTH: 0.5m COMPACTION: —

∴∵ sand
≡ clay

SEDIMENTARY TEXTURE AND STRUCTURES							% SAND				PHYSICAL CHARACTERISTICS					STRATIFICATION TYPE							SAMPLE					
CLAY	SILT	FINE SAND	MEDIUM SAND	COARSE SAND	GRAVEL	PEBBLE	INTERVAL (ft)	0	50	100	COLOR	DEFORMATION	BED THICKNESS	% SILT	% ORGANIC	% BIOTURBATION	WAVY	FLASER	LENTICULAR	CROSS BED	MASSIVE BED	INCLINED BED	HOR. LAMINAT.	GRAIN SIZE	HEAVEY MINERAL	MICRO FOSSILS	RADIOMETRIC	RADIOGRAPH	PHOTOTGRAPH

PHYSICAL DESCRIPTION:

0.0 – 0.17 m
Clay, brown, massive
purely clay for 1st 7-8 cm,
then steadily coarsens
before reaching max sand
content for approx 2 cm,
then abruptly transitions back
to clay at 17 cm depth.

0.17 – 0.32 m
clay, brown/gray, massive
exclusively clay in this layer
begins coarsening at 0.32m

0.32 – 0.5 m
sand-clay, brown/gray, massive
mostly sands
some clayeyer layers
coarsens towards bottom.

Note:
This core was intended to be
a full meter, but could
not penetrate below 0.5 m.
Presumably penetration was
blocked by a layer of sand.

(Depth markers: 0.0, 0.17m, 0.32m, 0.5)
(Color column: Brown or gray)

Figure A.5: Core MB-04

UNIVERSITY OF NEW ORLEANS
COASTAL RESEARCH LABORATORY
VIBRACORE DESCRIPTION SHEET

CORE ID: MB-05 DATE: 11-15-10 DESCRIBED BY: myke b.

ELEVATION: LOCATION: cubits gap

CORE LENGTH: 1.0 m COORDINATES: -89.1963 29.1876

TOTAL DEPTH: 1.0 m COMPACTION:

SEDIMENTARY TEXTURE AND STRUCTURES	% SAND	PHYSICAL CHARAC-TERISTICS	STRATI-FICATION TYPE	SAMPLE	PHYSICAL DESCRIPTION:

Color: BLACK OXIDATION / BROWN SANDS

% SILT Shells

PHYSICAL DESCRIPTION:

Top 10cm is missing

0.0 - 0.25
clay - little sand, brown color. massive bedding. Sub interval contains black organic fragments and is aqueous and unconsolidated. Bottom contactic abrupt but gradational.

0.25 - 0.37
sand, brown color, massive bedding. Sand is fine grained and moderatly compacted. bottom contact abrupt

0.37 - 0.50
clay, black brown, massive unconsolidated. sharp contact on bottom.

0.50 - 1.0 m
clay-sand, brown black color, massive bedding. sub unit is caped with a 4cm layer of brown fine grain sand. Below that, sediments are jumbled and alternate from sand and clay. Also the subunit is highly oxidized from 0.77-.93 m sugesting broken down organics.

Figure A.6: Core MB-05

Vita

Christopher Esposito comes to the University of New Orleans from Rutgers University where he earned a Bachelor's Degree in 2003, double majoring in Mathematics and Physical Oceanography. He arrived in New Orleans in 2007 as a high school teacher, and spent time developing an environmental sciences program for adjudicated youth in rural Louisiana before pursuing a Master's Degree under Dr. Ioannis Georgiou. He will be continuing his studies in the Earth Sciences at Tulane University beginning in the fall of 2011.